

# Design and Assessment of Membrane-supported Ammonia Cracking for Hydrogen Refuelling Stations

by

Emily Helen Smyth

A thesis  
presented to the University of Waterloo  
in fulfillment of the  
thesis requirement for the degree of  
Master of Applied Science  
in  
Chemical Engineering

Waterloo, Ontario, Canada, 2025

© Emily Helen Smyth 2025

## **AUTHOR'S DECLARATION**

I hereby declare that I am the sole author of this thesis. This is a true copy of the thesis, including any required final revisions, as accepted by my examiners. I understand that my thesis may be made electronically available to the public.

# Abstract

As Canada aims to reduce greenhouse gas emissions, there is a growing shift toward cleaner energy and fuel sources. Hydrogen has emerged as a promising alternative fuel source due to its high gravimetric energy density and ability to power fuel cell electric vehicles without producing direct carbon dioxide emissions. However, there are currently challenges in storing and transporting large amounts of hydrogen. Ammonia is gaining attention as a hydrogen carrier because it can be stored under moderate pressure or refrigeration and leverages existing infrastructure. Once delivered, hydrogen can be extracted from ammonia through on-site decomposition and purification. Although this pathway shows promise, its competitiveness depends on the system's energy requirements, operating costs and emissions. Furthermore, most existing ammonia decomposition and hydrogen refuelling models are proprietary, limiting accessibility for researchers and small-scale developers.

This thesis addresses this gap by developing an open-source process model for a palladium membrane-supported ammonia decomposition process at hydrogen refuelling stations. The process delivers 500 kg of hydrogen gas at 350 bar per day, and its cost and emissions performance were compared to other hydrogen production pathways. A Python-based model was created using Cantera, a chemical kinetic and thermodynamic library, to simulate the isothermal Pd membrane reactor. In the reactor, ammonia decomposes to nitrogen and hydrogen, while hydrogen is separated using the membrane. This eliminates the need for additional hydrogen purification steps. The base case achieved 99.92% conversion and 95.9% hydrogen recovery. To preheat the ammonia feedstock to the membrane reactor, the unconverted ammonia and unrecovered hydrogen were mixed with some ammonia feedstock and combusted with air. The combustion generates  $\text{NO}_x$  emissions, which were reduced by 85% using a selective catalytic reduction unit, bringing  $\text{NO}_x$  emissions well below provincial limits. While the system has no direct carbon dioxide emissions, indirect emissions from electricity consumption, ammonia feed and transportation for the process were estimated at 4.86 kg  $\text{CO}_2\text{e}/\text{kg H}_2$ , with an electricity requirement of 9.77 kWh/kg  $\text{H}_2$ . An economic analysis shows a capital expenditure of approximately \$204,000 and an annual operating cost of \$1.6 million for the base case. The levelized cost of hydrogen (LCOH) at 350 bar was estimated at \$10.38 kg/ $\text{H}_2$ . A sensitivity analysis was also conducted to evaluate the impact of temperature, pressure and membrane permeance on conversion, hydrogen recovery,  $\text{NO}_x$  emissions, and LCOH. The impact of capital and operating expenditure on LCOH was also analyzed, with the price of ammonia being the main contributor to changes in LCOH. These results from a detailed study of the ammonia to hydrogen pathways contribute to a better understanding of clean hydrogen technologies for transportation applications and also provide key insights for future deployment in clean fuel strategies across Ontario and beyond.

# Acknowledgements

First and foremost, I would like to thank my supervisor, XiaoYu Wu, who has provided invaluable guidance, support and encouragement over the past two years. Their expertise and mentorship have played a critical role not only in shaping the direction and quality of my research but also in fostering my academic and personal growth.

I would also like to thank my committee members, Dr. Aiping Yu and Dr. Eric Croiset, for generously offering their time, expertise and constructive feedback. Their thoughtful comments and suggestions have been instrumental in strengthening my thesis.

To my colleagues in the Greener Production Group, thank you not only for your support during the research process but also for the memorable board game nights, bowling, and thoughtful conversations that helped make this experience both enjoyable and meaningful. I feel fortunate to have been part of such an amazing research group.

Finally, I would like to thank my family for their continuous support and encouragement. Your encouragement, understanding, and belief in me provided the foundation I needed to persevere through the ups and downs of this journey. I could not have reached this milestone without you by my side.

# Table of Contents

AUTHOR’S DECLARATION .....	ii
Abstract .....	iii
Acknowledgements .....	iv
List of Figures.....	vii
List of Tables .....	ix
List of Abbreviations.....	x
List of Symbols.....	xi
Chapter 1 Introduction .....	1
1.1 Overview and motivation .....	1
1.2 Thesis outline.....	2
Chapter 2 Literature Review .....	3
2.1 Fundamentals.....	3
2.1.1 Hydrogen .....	3
2.1.2 Ammonia.....	3
2.1.3 Ammonia and hydrogen storage .....	3
2.1.4 Hydrogen refuelling stations.....	4
2.2 Ammonia decomposition .....	5
2.2.1 Kinetics.....	5
2.2.2 Catalyst.....	6
2.2.3 Membranes .....	6
2.2.4 Ammonia decomposition reactor technology.....	7
2.3 Ammonia Combustion and SCR.....	9
2.3.1 Ammonia Combustion.....	9
2.3.1 Selective catalyst reduction .....	11
2.4 Techno-economic and environmental considerations .....	12
2.4.1 Capital and operating cost .....	12
2.4.2 Levelized cost of hydrogen.....	13
2.4.3 NO <sub>x</sub> emissions standards and regulatory context.....	13

2.4.4 CO <sub>2</sub> emissions standards and regulatory context .....	14
2.4 Existing models and simulations .....	15
Chapter 3 Methodology .....	17
3.1 Process Description.....	17
3.2 Model Development.....	18
3.2.1 Software and computational tools.....	18
3.2.2 Governing Equations.....	18
3.3 Model set up and validation.....	24
3.3.1 Reactor Validation .....	24
Chapter 4 Base Case Results .....	29
4.1 Reactor Results .....	29
4.2 Process mass and energy balance .....	35
4.3 Economic Analysis .....	41
4.4 Environmental analysis.....	46
Chapter 5 Sensitivity Analysis .....	50
5.1 Impact of process variables on system outputs.....	50
5.2.1 Pressure .....	50
5.2.2 Temperature .....	53
5.2.3 Membrane Permeance .....	55
5.2 Sensitivity analysis on NO <sub>x</sub> emissions.....	58
5.3 Sensitivity analysis of the levelized cost of hydrogen .....	59
Chapter 6 Conclusions and Recommendations .....	62
5.1 Conclusion .....	62
5.2 Limitations of the Study and Recommendations of Future Work .....	63
References.....	65
Appendix A .....	72

# List of Figures

Figure 2.1: The current location of hydrogen refuelling stations in the US and Canada available to the public [18].	5
Figure 2.2: General membrane reactor diagram.	7
Figure 2.3: Schematic of a packed bed reactor for ammonia decomposition.	8
Figure 2.4: Schematic of membrane reactors for ammonia decomposition.	8
Figure 3.1: Ammonia decomposition process flow diagram with MR.	18
Figure 3.2: Small-scale PBR results from Kogekar [36] vs current model.	26
Figure 3.3: Packed bed reactor with and without membrane Kogekar [36] vs current model.	27
Figure 3.4: PBR species coverage (300 SCCM, 5 bar, 450°C).	28
Figure 4.1: Temperature profile along the length of the reactor under (a) adiabatic and (b) isothermal conditions.	30
Figure 4.2: Flow rate along the length of the reactor under (a) adiabatic and (b) isothermal conditions.	31
Figure 4.3: Ammonia decomposition reactor overall retentate flowrate.	32
Figure 4.4: Ammonia decomposition reactor surface chemical species mass fraction.	33
Figure 4.5: Pressure drop over the membrane reactor.	33
Figure 4.6: Process flow diagram for ammonia decomposition.	35
Figure 4.7: Process code diagram for ammonia decomposition.	36
Figure 4.8: Sankey diagram of mass flow through the ammonia decomposition process, (a) entire process and (b) excluding air used in heat exchangers.	38
Figure 4.9: Energy flow through ammonia decomposition process.	40
Figure 4.10: Equipment Cost Breakdown.	41
Figure 4.11: LCOH breakdown.	45
Figure 4.12: Electricity consumption of hydrogen production paths.	47
Figure 4.13: CO <sub>2</sub> -equivalent emissions per kilogram of hydrogen for various production methods (Appendix A Table A.8).	48
Figure 5.1: Influence of retentate pressure on hydrogen recovery (permeate side pressure is kept at 1 bar).	51
Figure 5.2: Influence of pressure on ammonia conversion.	52
Figure 5.3: Influence of pressure on electricity consumption.	52
Figure 5.4: Influence of temperature on hydrogen recovery.	53
Figure 5.5: Influence of temperature on ammonia conversion.	54
Figure 5.6: Influence of temperature on electricity consumption.	55

Figure 5.7: Influence of membrane permeance on hydrogen recovery.....	56
Figure 5.8: Influence of membrane permeance on ammonia conversion. ....	57
Figure 5.9: Influence of membrane permeance on energy consumption. ....	58
Figure 5.10: Influence of equivalence ratio on NO <sub>x</sub> and N <sub>2</sub> O concentration. ....	59
Figure 5.11: Impact of ±30% variations in capital and operating cost parameters on the Levelized Cost of Hydrogen (LCOH).....	60
Figure 5.12: Effect of key parameters of LCOH.....	61

# List of Tables

Table 2.1: Operating parameters and performances of packed bed membrane reactor (PBMR) vs packed bed reactor (PBR). .....	9
Table 2.2: Equivalence ratio for combustion meaning [43]. .....	10
Table 2.3: NO <sub>x</sub> emission limit for boilers and heaters in Ontario [53]. .....	13
Table 2.4: NO <sub>x</sub> emission limits expressed in ppm NO <sub>x</sub> by volume in the flue gas at 3% O <sub>2</sub> in the flue gas, dry basis [53]. .....	14
Table 2.5: Ontario's electricity source [55]. .....	14
Table 3.1: Catalyst mechanism Ni-BCZYBYB [58]. .....	20
Table 3.2: Small-scale ammonia decomposition reactor parameters. ....	25
Table 4.1: Large-scale ammonia decomposition membrane reactor parameters. ....	30
Table 4.2: Reactor summary of outlet stream. ....	34
Table 4.3: Summary of parameters used for the system. ....	37
Table 4.4: Assumptions applied for LCOH estimation in the base case. ....	42
Table 4.5: Estimation of total capital investment cost [50]. .....	43
Table 4.6: Estimation of total production cost. ....	44
Table 4.7: Ambient Air Quality Criteria NO <sub>2</sub> and N <sub>2</sub> O [41]. ....	49
Table 4.8: Base case results for NO <sub>x</sub> emissions. ....	49
Table 5.1: Parameters and values used in the sensitivity analysis. ....	50
Table A.1: Base case stream results. ....	72
Table A.2: Base case pump results Python model vs the Aspen Plus model. ....	73
Table A.3: Base case heat exchanger with phase change results Python model vs the Aspen Plus model. ....	73
Table A.4: Base case heat exchangers (Ex: HX4) results Python model vs the Aspen Plus model. ....	73
Table A.5: Base case multistage compressor results Python model vs the Aspen Plus model. ....	74
Table A.6: Base case ammonia combustion results Python model vs the Aspen Plus model. ....	74
Table A.7: Energy Consumption for hydrogen production processes. ....	74
Table A.8: CO <sub>2</sub> emissions for hydrogen production processes. ....	75
Table A.9: Total Equipment Cost (CAD). ....	75

# List of Abbreviations

CAPEX	Capital expenditure
CRF	Cost recovery factor
FCEV	Fuel cell electric vehicles
HRS	Hydrogen refuelling station
LCOH	Levelized cost of hydrogen
NC	Number of constituents
NP	Number of products
OPEX	Operational expenditure
PBMR	Packed bed membrane reactor
PBR	Packed bed reactor
PSA	Pressure swing adsorption
ROI	Return on investment
SCR	Selective catalyst reduction
SMR	Steam methane reforming
TCI	Total capital investment
TSA	Temperature swing adsorption

# List of Symbols

$\beta$	Pressure ratio
$\beta_g$	Packed-bed permeability
$\Gamma$	Surface density (mol/cm <sup>2</sup> )
$\gamma_i$	Collision frequency
$\delta_{k,kM}$	Kronecker delta (=1 for membrane species, =0 for non-membrane species)
$\varepsilon_{k,i}$	Coverage dependent activation energy corresponding to the kth species in the ith heterogeneous reaction.
$\eta$	Efficiency
$\theta_k$	Surface coverage species k
$\mu$	Viscosity (Pa s)
$\mu_{cp}$	Chemical potential
$\nu$	Stoichiometric coefficient
$\xi$	Extent of reaction
$\rho$	Density (kg/m <sup>3</sup> )
$\tau_g$	Tortuosity
$\phi$	Equivalence ratio
$\phi_g$	Porosity gas phase
$\dot{\omega}_k$	Net production rate of gas-phase species k (kmol/m <sup>3</sup> /s)
$A$	The pre-exponential factor
$A_b$	Cross-sectional area of reactor (m <sup>2</sup> )
$A_r$	Area (m <sup>2</sup> )
$A_s$	Specific area (1/m)
$B_{kM}$	Membrane permeability (kmol/m s Pa)
$b$	The temperature exponent
$C$	Equipment cost (CAD)
$C_p$	Specific heat capacity at constant pressure (J/mol K)
$D_p$	Particle diameter (m)
$E_a$	Activation energy of reaction i (J/mol K)
$G$	Gibbs free energy (J/mol)
$H$	Enthalpy (J/mol)
$h$	Partial enthalpy (J/mol)

$\hat{h}$	Heat transfer coefficient (W/m <sup>2</sup> K)
$h_{kM}$	Partial enthalpy of membrane species (KJ/mol)
$h_{latent}$	Latent heat of vaporization (kJ/kg)
$I$	Cost index
$i$	Discount rate (%)
$j_{kM}$	Mass flux of species k (kg/m <sup>2</sup> s)
$k_i$	Reaction rate constant
$k'_i$	Modified rate constant for species i
$m$	Number of adsorption sites
$\dot{m}$	Mass flowrate (kg/s)
$N$	Number of stages
$n$	Number of moles
$n_{pl}$	Plant life (years)
$p_{kM,mem}^\alpha$	Perm-selective species partial pressure packed-bed (Pa)
$p_{kM,sweep}^\alpha$	Perm-selective species partial pressure exterior sweep channel (Pa)
$P$	Power (kW)
$P_b$	Perimeter of reactor (m)
$p$	Pressure (Pa)
$p_{int,i}$	Intermediate stage pressure for stage i (Pa)
$p_{st}$	Storage pressure (Pa)
$Q$	Heat (W)
$R$	Universal gas constant
$s'_k$	Net production rate of surface-phase species k (kmol/m <sup>2</sup> /s)
$T$	Temperature (K or °C)
$T_w$	Wall temperature (K)
$\Delta T_{lm}$	Log mean temperature
$t_m$	Membrane thickness (m)
$U$	Internal energy (W)
$U_{HX}$	Overall heat transfer coefficient (W)
$u$	Specific velocity (m/s)
$V$	Volume (m <sup>3</sup> )
$W_k$	Molecular weight of gas-phase species k (kg/kmol)
$w_{is}$	Specific work (isentropic) (W)

$Y_k$	Mass fraction of species k
$Z_k$	Surface concentration
$z$	Length of reactor (m)

# Chapter 1 Introduction

## 1.1 Overview and motivation

Currently, Canada has a goal of becoming net-zero emissions by 2050. Therefore, it is important that Canada's economy is powered by clean power and clean fuels to meet this goal [1]. In 2023, the transportation sector was the country's second-largest source of greenhouse gas (GHG) emissions, contributing to approximately 23% of the total emissions [2]. The amount released was 157 megatons of CO<sub>2</sub> equivalent [2]. Since 1990, the emissions from the transportation sector have increased by 33% due to an increase in population and demand [2]. This trend is expected to grow as Canada tries to support the increasing population in the coming decades. Therefore, efforts must be directed toward decarbonizing this sector. One solution is using clean fuels such as hydrogen. As the global hydrogen market value is expected to reach as much as \$1.9 trillion by 2050, and Canada has the potential to produce large amounts of low-cost, clean hydrogen to meet its domestic demand, it creates an opportunity for Canada to become a supplier of choice of a new carbon-free energy export commodity [3].

In 2020, Canada launched a call to action to harness the potential of hydrogen to benefit the country and its people [4]. From this, a framework was created to focus on low-carbon hydrogen as a tool to achieve our goal of net-zero emissions by 2050 [4]. A progress report was released for Canada's Hydrogen Strategy framework, which highlights all major developments across the hydrogen value chain and any recommendations that need to be made for this framework [4]. Hydrogen has been the main focus for clean energy systems because of its high gravimetric energy density compared to other fuel sources. Hydrogen has a high gravimetric energy density of 120 MJ/kg [5], which is slightly more than twice that of methane (55.6 MJ/kg) and more than twice that of gasoline (46 MJ/kg). This also makes it ideal as hydrogen carries more energy for the same substance. This is ideal for applications where weight matters, such as aerospace, heavy transport and portable power. In addition, when hydrogen is used in FCEV, the only byproduct is water; therefore, there are no direct carbon dioxide emissions. However, despite its high energy per kilogram, hydrogen's low volumetric density compared to other liquid fuels like diesel and gasoline remains a major challenge for storage and transportation. Hydrogen is typically stored at either high-pressure compressions (350 or 700 bar, ambient temperature), liquefaction at cryogenic temperatures (1 atm, -253°C) or advanced material-based storage (like metal hydrides)[6]. Each of these methods has high energy costs, complexity and safety risks. In addition to the storage challenges, there are also challenges with other current infrastructure, such as pipelines, transportation and distribution [7]. For pipelines, there are concerns

with hydrogen embrittlement (where hydrogen diffuses into steel); therefore, more expensive materials are needed, which increases the cost of installing pipelines to transport hydrogen long distances[8]. Current transportation and distribution systems for fuels are not suitable for use with hydrogen, as they were designed for substances with different physical and chemical characteristics. Even with retrofitting these existing infrastructures or building new infrastructure, it requires a massive investment and must meet strict safety standards [9].

As the use of hydrogen increases, ammonia is rapidly gaining recognition as a leading solution for hydrogen storage and transportation. Ammonia can be stored as a liquid under moderate pressure or refrigeration and transported using existing infrastructure such as tanks and pipelines. It also benefits from an established global production and distribution network, which helps lower long-term storage and handling costs. Once delivered, hydrogen can be released from ammonia through on-site decomposition, allowing for a decentralized hydrogen supply for refuelling stations without relying on large, high-pressure or cryogenic storage systems. Using ammonia cracking is a promising solution for decentralized hydrogen distribution; however, its end use highly depends on factors such as energy input, operating costs, emissions intensity, and integration with renewable energy sources. In addition, most modelling tools available for ammonia decomposition and hydrogen refuelling are proprietary and lack transparency, restricting their accessibility for researchers, policymakers, and smaller-scale project developers. This research addresses that gap by developing an open-source model for the ammonia-to-hydrogen conversion process at refuelling stations and comparing its emissions and cost to other hydrogen production methods. The objectives are to simulate the process using publicly available tools, evaluate its economic and environmental performance, conduct a sensitivity analysis to identify key influencing parameters, and compare the ammonia-based system to other hydrogen production methods such as electrolysis and steam methane reforming (with and without carbon capture). By focusing on open-access modelling, this work aims to support broader adoption and informed decision-making for future hydrogen infrastructure.

## **1.2 Thesis outline**

The following sections of the thesis are structured as follows: Chapter 2 presents a literature review, offering background on ammonia decomposition and key concepts in chemical process cost analysis. Chapter 3 outlines the development and validation of the simulation model. Chapter 4 discusses the results of the base case, including process performance, emissions, and economic evaluation. Chapter 5 explores the sensitivity of various process parameters and their impact on overall costs and environmental outcomes. Finally, Chapter 6 provides a summary of the findings and offers recommendations based on this thesis.

# Chapter 2 Literature Review

## 2.1 Fundamentals

### 2.1.1 Hydrogen

Hydrogen is the most abundant chemical element in the universe and typically exists in its molecular form ( $H_2$ ). Under standard conditions, it is a colourless, odourless, non-toxic, and highly combustible gas. Although rarely found in its elemental form in nature, hydrogen is widely present in compounds such as water ( $H_2O$ ), ammonia ( $NH_3$ ), and hydrocarbons. This abundance allows hydrogen to be produced from a variety of feedstocks through processes such as electrolysis, steam methane reforming, and ammonia cracking. While hydrogen is usually found as a gas, it can be liquefied under cryogenic conditions at extremely low temperatures ( $-253^\circ C$ ) for storage and transport [6]. Hydrogen has a lower heating value (LHV) of approximately 120 MJ/kg and a higher heating value (HHV) of around 142 MJ/kg, making it an energy-dense fuel on a mass basis [5]. As hydrogen has a high energy content, it is a promising energy carrier that can help in the transition towards cleaner energy systems.

### 2.1.2 Ammonia

Ammonia ( $NH_3$ ) is a chemical compound composed of nitrogen and hydrogen. It is a colourless gas at room temperature and has a strong odour. Ammonia plays an important role in various industrial and household applications, most notably as a key ingredient in the production of fertilizers and in cleaning products, refrigeration systems, and wastewater treatment. It has a boiling point of  $-33.3^\circ C$ , which allows it to be stored and transported under moderate pressure or temperature when compared to hydrogen. Ammonia is essential to many everyday applications; however, it can be hazardous in high concentrations. In humans, it can affect the respiratory system, and if ammonia is released into the environment, it can be harmful to the aquatic ecosystem. Therefore, it is important to have strict safety measures when handling ammonia. Given its high hydrogen content and existing infrastructure, ammonia is gaining attention as a potential hydrogen carrier [10],[11].

### 2.1.3 Ammonia and hydrogen storage

The storage of hydrogen and ammonia has its challenges and trade-offs that influence the design and deployment of hydrogen energy systems. Hydrogen is typically stored in three primary forms: compressed gas, cryogenic liquid, and solid-state storage. Compressed hydrogen gas is generally stored at 350 or 700 bar. This is a very energy-intensive process; however, it is the most widely used in mobility applications such as fuel cell electric vehicles. Due to hydrogen, low volumetric energy

density (even under high pressure) poses challenges for long-distance transportation and large-scale storage. Hydrogen can also be stored in a cryogenic liquid state at  $-253^{\circ}\text{C}$  under atmospheric pressure [12]. This significantly increases the volumetric density; however, liquefaction is highly energy-intensive (roughly 30-40% of the energy content of the hydrogen itself) and requires advanced insulation to reduce boil-off losses during storage and transport. Finally, hydrogen can be absorbed or adsorbed into metal hydrides or porous materials. Although these methods offer safety and compactness, they are currently less commercially viable due to weight, cost, and slow kinetics. Another consideration for hydrogen storage is the material compatibility, especially as hydrogen can cause embrittlement in metals. Hydrogen also has a wide flammability range (4-75% in air) and low ignition energy demand; therefore, there needs to be strict leak prevention and detection [13].

Ammonia is typically stored as a liquid at moderate pressure, 10-15 bar, at  $20^{\circ}\text{C}$  or refrigerated at atmospheric pressure ( $-33.3^{\circ}\text{C}$ ). These conditions are much less extreme than those required for liquid hydrogen, resulting in reduced insulation and compression costs. As a result, existing infrastructure from the fertilizer and chemical industries can be leveraged for ammonia storage and transport [14]. The main types of tanks that are used for storing under atmospheric conditions are single-wall steel tanks with external insulation or steel tanks with double walls and perlite insulation in between the walls [15].

#### **2.1.4 Hydrogen refuelling stations**

Hydrogen refuelling stations (HRS) play a vital role in enabling the use of fuel cell electric vehicles (FCEVs), and ammonia has emerged as a promising hydrogen carrier for supplying these stations. Ammonia can be cracked on-site to produce hydrogen, offering an alternative to conventional off-site hydrogen delivery methods. In an off-site HRS, hydrogen is generated at a centralized facility and transported to the station. In contrast, in an on-site HRS, hydrogen is produced locally, potentially via ammonia decomposition. On-site ammonia cracking can reduce transportation costs and improve station flexibility, but it may face challenges such as limited land availability for installing reactors and purification systems. A typical HRS includes a hydrogen storage system, a cooling unit, and a dispenser equipped with a nozzle that interfaces with FCEVs. To meet fueling requirements, stations must be capable of dispensing hydrogen at a minimum of 350 bar for medium- and heavy-duty vehicles, and 700 bar for light-duty vehicles [16]. While the early focus of proton exchange membrane fuel cells (PEMFCs) was on light-duty vehicles, there has been a shift toward heavy-duty applications, such as trucks, buses, trains, and ships, due to their higher energy demands, longer lifespans, and predictable routes that simplify refuelling logistics [17].

Globally, there are now over 1,000 hydrogen refuelling stations in operation, with many more in the planning stages. However, most are located in Europe and Asia, particularly in China, South Korea, and Japan. Currently, the US and Canada remain underdeveloped in hydrogen infrastructure. Most hydrogen refuelling stations are located in California, and only a few Canadian stations are available to the public in British Columbia and Quebec. Figure 2.1 shows the current location of HRS in the US and Canada. This limited infrastructure poses a major barrier to the widespread adoption of hydrogen-fueled FCEVs in the region [18].



Figure 2.1: The current location of hydrogen refuelling stations in the US and Canada available to the public [18].

Hydrogen demand for heavy-duty trucks is significant, with consumption rates ranging from 7.7 to 9.04 kg per 100 km, and refuelling is required after journeys of approximately 500 km [19],[20],[21],[22]. More reliable and accessible refuelling stations need to be built to use hydrogen as a fuel. Therefore, it is important to evaluate ammonia's role as a hydrogen carrier for on-site hydrogen production.

## 2.2 Ammonia decomposition

### 2.2.1 Kinetics

Ammonia decomposition is a well-studied reaction due to its relevance in hydrogen production. It is the process of breaking down ammonia into nitrogen and hydrogen. The overall reaction is as follows:



Ammonia decomposition generally follows a stepwise mechanism involving adsorption, dissociation and desorption [23]. This reaction is endothermic and becomes thermodynamically favourable at high temperatures (typically above 400°C) [24].

The decomposition of ammonia was first studied in the early 20th century, primarily in understanding gas-phase chemical reactions and catalysis. A German chemist, Fritz Haber, who studied the ammonia synthesis process (the Haber-Bosch process), also laid the groundwork for exploring its reverse reaction [25]. As the demand for hydrogen as a clean fuel source increases, ammonia decomposition has been revisited as a promising route for on-demand hydrogen generation. This would be used for fuel cells and portable hydrogen applications.

### **2.2.2 Catalyst**

Ammonia decomposition is the reverse of the Haber-Bosch synthesis process. Following the principle of microreversibility, initial studies explored the use of traditional synthesis catalysts, such as Fe and Ru. However, more research has expanded to include Ru-based and a wide variety of transition metal catalysts (e.g., Ni, Mo, Co, Ir, Pt, Pd, Rh), as well as multi-metal combinations [26].

From all the studied catalysts, Ru-based materials show the highest catalytic activity, especially when supported on oxide or carbon-based materials. However, the high cost and environmental impact of noble metals like Ru have prompted a shift toward low-cost alternatives such as Fe, Ni, and Co. Currently, Ni supported on alumina is widely used in the industry due to its thermal stability, cost-effectiveness, and durability. Catalytic performance is influenced not only by the active phase but also by the support material and promoters. High surface area supports and basic materials (e.g., MgO, Al<sub>2</sub>O<sub>3</sub>, CeO<sub>2</sub>) enhance metal dispersion and electron donation, which improve activity. Promoters like K, Cs, and Ba further boost activity by altering the electronic environment and stabilizing active phases. The reaction gas composition also affects catalyst behaviour along the reactor bed, with varying NH<sub>3</sub>, H<sub>2</sub>, and N<sub>2</sub> concentrations shifting the optimal performance conditions. Sustainability considerations now include not only performance and cost but also factors like global warming potential (GWP) and the energy intensity of metal extraction [26].

### **2.2.3 Membranes**

The most used hydrogen-selective membranes are dense metallic membranes, particularly those made of palladium (Pd) or Pd-based alloys. These membranes operate based on a solution–diffusion mechanism, where molecular hydrogen dissociates into atoms on the high-pressure (retentate) side, diffuses through the metal lattice, and recombines into H<sub>2</sub> molecules on the low-pressure (permeate)

side. This mechanism allows for nearly perfect hydrogen selectivity and ultra-high purity (exceeding 99.999%) [27]. Alternative materials such as ceramic or porous inorganic membranes (e.g., silica, zeolite, and perovskites) have also been studied for hydrogen separation. While they are more thermally stable and chemically robust than polymeric membranes, they generally exhibit lower hydrogen selectivity than Pd-based membranes. They may require functionalization or thin selective layers to achieve acceptable performance [28].

In ammonia decomposition, hydrogen-selective membranes are integrated into membrane reactors to improve hydrogen yield and reduce the need for downstream purification. In Figure 2.2, it shows a membrane reactor used for ammonia decomposition, where the permeable gas is selectively removed through a permeable membrane. Inside the reactor tube, the reaction takes place. The permeable gas then diffuses through the membrane into the outer shell, driven by a pressure gradient or sweep gas. This continuous removal of the permeable gas shifts the reaction equilibrium, improving conversion efficiency while simultaneously producing high-purity gas, eliminating the need for an extra purification system.

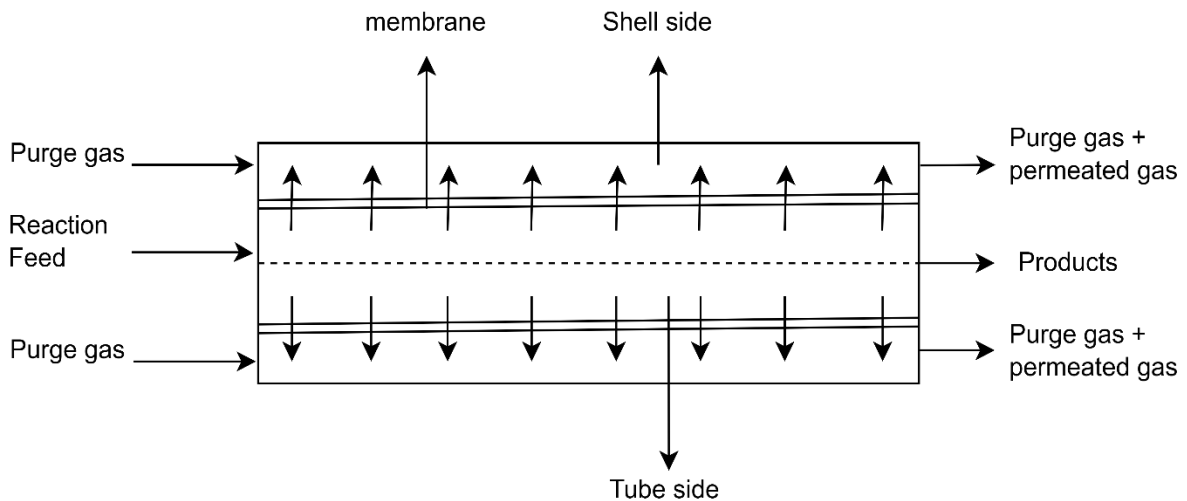


Figure 2.2: General membrane reactor diagram.

## 2.2.4 Ammonia decomposition reactor technology

Ammonia decomposition is the most important part of the ammonia to hydrogen process. This process efficiency depends on the catalyst being used and the type of hydrogen separation method that is employed. Reactors for ammonia decomposition can be categorized into non-membrane (conventional) reactors or membrane reactors. For purification technology, either membranes or pressure swing adsorption (PSA) columns can be used to separate and obtain pure hydrogen.

Packed bed reactors are the most conventional technology for ammonia decomposition, and as mentioned in the previous section, the reaction is typically carried out over a Ni catalyst bed. This is then followed by a PSA process to remove hydrogen, but it can also be achieved using temperature swing adsorption (TSA)[24]. Figure 2.3 shows a simplified schematic of a packed bed reactor.

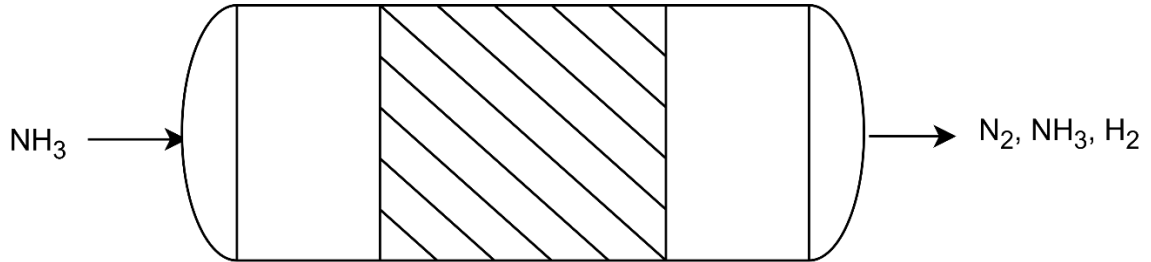


Figure 2.3: Schematic of a packed bed reactor for ammonia decomposition.

Membrane reactor technology combines the ammonia decomposition and hydrogen purification steps into a single compact unit [24]. Using this reactor selectively removes hydrogen that can both decrease the operating temperature, and there is a much greater hydrogen productivity when compared to a packed bed reactor (PBR). Figure 2.4 shows a schematic of a PBMR for ammonia decomposition, where the retentate is on the inside and the permeate is on the outside. This configuration can change by having the permeate on the inside and the retentate on the outside.

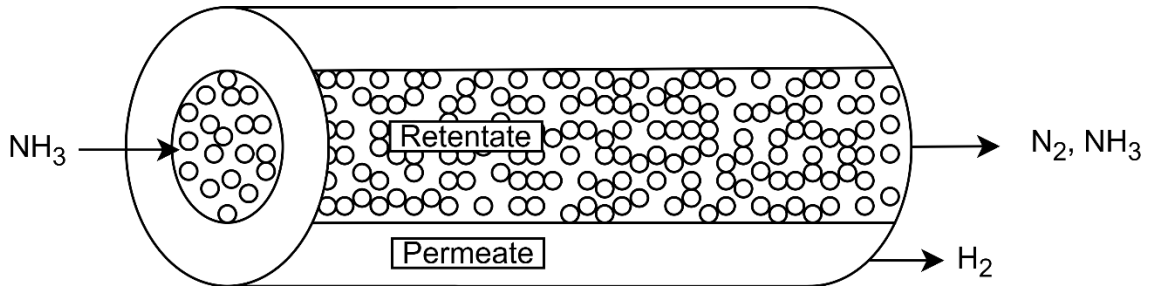


Figure 2.4: Schematic of membrane reactors for ammonia decomposition.

While both reactor types aim to maximize hydrogen production, their design, operation and separation strategies are slightly different. Table 2.1 summarizes and compares the typical operating conditions, hydrogen recovery, and separation processes associated with PBMRs and PBRs as reported in the literature.

Table 2.1: Operating parameters and performances of packed bed membrane reactor (PBMR) vs packed bed reactor (PBR).

Operating condition/type	PBMR	PBR
Temperature (°C)	400-600 [29], [30], [31], [32]	400-800 [33], [29], [30], [31], [32]
Reactor (Retentate)	1-25 [29],[30],[31],[32]	1-25 [29], [30], [31], [32]
Pressure (bar)		
Permeate Pressure (bar)	0.01-1 [31], [32], [34]	-
Separation Process	Pd-Membrane [29],[30],[35]	Pressure swing adsorption (PSA) [29], [30]
Hydrogen Recovery (%)	95 [29],[30]	85 [29],[30]
Bed Porosity	0.4-0.6 [32], [36], [37], [38]	
Permeance ( $\frac{kmol}{m^2 s Pa}$ )	-6.46e-10 – 2.32e-9 [35], [39]	-

## 2.3 Ammonia Combustion and SCR

### 2.3.1 Ammonia Combustion

To reduce carbon dioxide (CO<sub>2</sub>) emissions from traditional hydrocarbon fuels, ammonia (NH<sub>3</sub>) is increasingly being investigated as a carbon-free alternative fuel. Unlike fossil fuels, ammonia combustion does not produce CO<sub>2</sub>; however, it poses challenges due to the potential for increased emissions of nitrogen oxides (NO<sub>x</sub>), which are potent pollutants and contribute to smog and acid rain. The primary chemical reaction for the stoichiometric combustion of ammonia in oxygen is [41]:



This reaction is highly exothermic and ideally produces only nitrogen and water vapour. However, real combustion systems are far more complex. In practical scenarios, a range of intermediate and side reactions occur, especially at high temperatures, leading to the formation of various NO<sub>x</sub> species (NO and NO<sub>2</sub>).

Ammonia's narrow flammability limits, high ignition temperature (~650°C), and low laminar burning velocity (~7 cm/s) make it more difficult to combust compared to traditional fuels [42]. Therefore, many studies investigate co-firing ammonia with hydrogen or using advanced burner designs to improve flame stability and reduce NO<sub>x</sub> emissions. Devkota et al.[43] observed that furnace efficiency and exhaust gas temperature decrease with increasing excess air. While excess air can help reduce NO<sub>x</sub> formation by lowering the flame temperature, it also dilutes the reactants and products, reducing thermal efficiency. Excess air is quantified using the following relation [43]:

$$\text{Excess air} = \frac{(\text{moles of air})_{\text{fed}} - (\text{moles of air})_{\text{theoretical}}}{(\text{moles of air})_{\text{theoretical}}} \times 100 \quad (3)$$

In actual furnace or combustor operation, achieving perfect adiabatic conditions is challenging due to heat losses, wall effects, and mixing inefficiencies. These factors lower the effective flame temperature and may lead to incomplete ammonia conversion, with traces of unburned NH<sub>3</sub> or intermediate nitrogenous species in the exhaust. The formation of NO<sub>x</sub> is susceptible to temperature, pressure, oxygen availability and fuel blending.

The equivalence ratio is a dimensionless parameter used in combustion analysis to describe the ratio of fuel to oxidizer in a combustion mixture relative to the stoichiometric (ideal) ratio. The equivalence ratio ( $\phi$ ) is important because it directly influences combustion performance, efficiency, and emissions. Understanding and controlling the equivalence ratio allows engineers and scientists to optimize combustion systems for fuel utilization, environmental impact, and thermal efficiency. The following equation is used to calculate the equivalence ratio [43]. Table 2.2 describes the type of equivalence ratio values and their meaning.

$$\phi = \frac{\text{stoichiometric air to fuel ratio}}{\text{actual air to fuel ratio}} \quad (4)$$

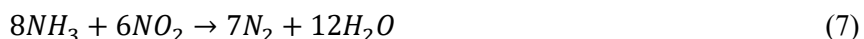
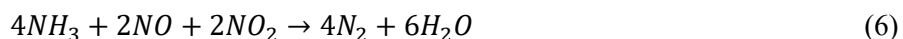
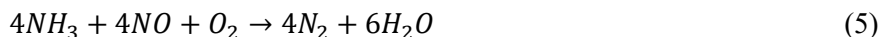
Table 2.2 describes the type of equivalence ratio values and their meaning.

Table 2.2: Equivalence ratio for combustion meaning [43].

<b>Condition</b>	<b>Description</b>
Lean combustion ( $\phi < 1$ )	More oxygen than needed.
Stoichiometric ( $\phi = 1$ )	Ideal ratio
Rich combustion ( $\phi > 1$ )	Excess fuel

### 2.3.1 Selective catalyst reduction

The selective catalyst reduction (SCR) process is a leading technology that removes nitrogen oxides from industrial and automotive exhaust gases. This technology has the advantages of high efficiency, low reaction temperature, and no secondary pollution. It operates by reacting ammonia with  $\text{NO}_x$  in the presence of a catalyst to produce nitrogen and water. Equations 5-7 show the three main reactions occurring:



The first reaction shown above is commonly referred to as the standard SCR reaction. In most exhaust gases,  $\text{NO}_x$  consists of over 90% NO that reacts with ammonia through this standard mechanism. The second reaction, also known as the fast SCR reaction, presents a promising strategy for improving efficiency in low-temperature regimes. This reaction, which involves an equimolar mixture of NO and  $\text{NO}_2$ , proceeds significantly faster than the standard SCR reaction when temperatures fall below  $300^\circ\text{C}$ . In contrast, the reaction described in reaction three is considerably slower when compared to the fast SCR reaction and even the standard reaction, thus limiting its effectiveness under similar conditions [44].

The performance of SCR depends on the choice of catalyst. Common catalyst types include V-based ( $\text{V}_2\text{O}_5\text{-WO}_3/\text{TiO}_2$  and  $\text{V}_2\text{O}_5\text{-MoO}_3/\text{TiO}_2$ ), Mn-based, Ce-based, and Fe-based metal oxides [45]. There is also a zeolite catalyst, which includes Cu-based zeolite catalyst (Cu-SSZ-13, Cu-SAPO-34) and Fe-based zeolite catalyst (Fe-ZSM-5, Fe-SSZ-13)[45]. Other special types of catalyst that can be used are spinel catalyst ( $\text{AB}_2\text{O}_4$ ) and perovskite catalyst [45]. Although vanadium-based catalysts are widely used, other catalysts are being considered, as at high temperatures,  $\text{V}_2\text{O}_5$  can be very toxic. SCR operate between  $150\text{-}450^\circ\text{C}$ , and according to recent literature,  $\text{NH}_3\text{-SCR}$  catalysts typically achieve  $\text{NO}_x$  conversion rates exceeding 90% under optimized conditions [45]. In some cases, such as with Ce-doped  $\text{LaMnO}_3$  or specially structured  $\text{MnCrO}_x$  catalysts, conversion rates of up to 100% have been reported at moderate temperatures ( $120\text{-}220^\circ\text{C}$ ) [45].

Due to several physical and chemical mechanisms, SCR catalyst performance can degrade over time. One of the main causes of deactivation is catalyst poisoning, which occurs when certain derived compounds, such as calcium oxide, magnesium oxide, potassium, sodium, arsenic, chlorine, fluorine, and lead, irreversibly occupy active sites within the catalyst. These compounds block the sites required for  $\text{NO}_x$  reduction. Another degradation mechanism is thermal sintering, which happens

from prolonged exposure to high flue gas temperatures. The thermal stress can also alter the catalyst's structure, affecting the surface area and activity. Blinding, plugging, and fouling are additional issues caused by the accumulation of particulate matter like fly ash or ammonia-sulphur salts on the catalyst surface. This can restrict gas flow and reduce the number of active sites available for the SCR reaction. Lastly, catalyst aging is another issue, which refers to the gradual decline in catalytic activity over time due to changes in the physical and chemical characteristics of the material, even under normal operating conditions [46].

Another consideration for SCR is ammonia slip, which refers to emissions of unreacted ammonia that result from the incomplete reaction of the  $\text{NO}_x$  and the reagent. Ammonia slip levels are typically 2 to 10 ppm, as at this level, ammonia does not result in plume formation or human health hazards [47].

## **2.4 Techno-economic and environmental considerations**

Evaluating the economic viability of a chemical process requires examining both capital and operating costs. This is done to compare different technologies and deployment strategies. In addition, this thesis will look into the levelized cost of hydrogen (LCOH), which provides a unified metric to compare hydrogen production trends on a consistent basis.

### **2.4.1 Capital and operating cost**

Capital cost refers to the upfront investment required to design, procure, construct, and commission a hydrogen production facility. For capital cost estimates, there are five generally accepted classifications, which are detailed estimate, definite estimate, preliminary estimate, study estimate and order-of-magnitude estimate. For this thesis, a study (also known as a major equipment or factored) estimate will be performed. This type of estimate lists the cost associated with all major equipment. This includes all pumps, compressors and turbines, columns and vessels, fired heaters, and exchangers. For this, each piece of equipment is roughly sized, and the cost is determined from this [48]. In addition to direct equipment costs, capital expenditures (CAPEX) also account for site preparation, infrastructure, installation labour, contingency, and engineering design.

Operating costs include all expenses incurred during the regular operation and maintenance of the process. This consists of feedstock cost (e.g., ammonia price), utilities (electricity, cooling water, fuel), labour, catalyst and membrane replacement, and maintenance.

## 2.4.2 Levelized cost of hydrogen

The LCOH is a key metric that represents the average cost per kilogram of hydrogen produced over the lifetime of a facility, taking into account both capital and operating costs. It allows fair comparison of different hydrogen production technologies (e.g., steam methane reforming, water electrolysis, ammonia cracking) under varying economic and operational conditions. LCOH is calculated by discounting all future costs and dividing the total by the amount of hydrogen produced over the system's lifetime. Factors influencing LCOH include plant lifetime, capacity factor, fuel cost, electricity price, conversion efficiency, and financing terms. In literature, Makhloufi et al.[49] modelled a large-scale fired ammonia cracker with an estimated LCOH of €5.65/kg H<sub>2</sub> (CAD \$9.03/kg H<sub>2</sub>) at 250 bar. Other studies, such as those from Nasharuddin et al.[33], Devkota et al. [50] and Lee et al. [19] have estimated the LCOH for ammonia decomposition without a membrane to be USD \$5.50/ kg H<sub>2</sub> (CAD \$7.54/kg H<sub>2</sub>), USD \$6.05/ kg H<sub>2</sub> (CAD \$8.30/kg H<sub>2</sub>), and USD \$6.27/ kg H<sub>2</sub> (CAD \$8.57/kg H<sub>2</sub>), respectively, at 1atm. For other hydrogen production methods, such as steam methane reforming and steam methane reforming with carbon capture systems, the LCOH can range from USD \$1.5-2.5/ kg H<sub>2</sub> (CAD \$2.06-3.43/kg H<sub>2</sub>) and USD \$2-3.50/ kg H<sub>2</sub> (CAD \$2.75-4.80/kg H<sub>2</sub>), respectively [51]. Comparing the LCOH across technologies and different production methods can highlight the trade-offs between cost and efficiency, which can help guide decision-makers towards cost-effective solutions

## 2.4.3 NO<sub>x</sub> emissions standards and regulatory context

NO<sub>x</sub> emissions refer to the various forms of nitrogen oxides that can be produced during ammonia combustion. This includes nitric oxide (NO) and nitrogen dioxide (NO<sub>2</sub>). These chemical compounds play a significant role in photochemical reactions that lead to smog formation and acid rain, which pose a significant risk to both health and the environment. In addition, another compound that is emitted during ammonia combustion is nitrous oxide (N<sub>2</sub>O), which, when emitted, has 273 times the 20-year global warming potential (GWP<sub>20</sub>) of CO<sub>2</sub> [52].

In Ontario, Canada, there are guidelines for NO<sub>x</sub> emissions from boilers and heaters. Table 2.3 and Table 2.4 show the NO<sub>x</sub> emission limits in Ontario for boilers and heaters.

Table 2.3: NO<sub>x</sub> emission limit for boilers and heaters in Ontario [53].

Capacity	Gaseous Fuel
10.5-105 GJ/h	26 g/GJ
>105 GJ/h	40g/GJ

Table 2.4: NO<sub>x</sub> emission limits expressed in ppm NO<sub>x</sub> by volume in the flue gas at 3% O<sub>2</sub> in the flue gas, dry basis [53].

Capacity	Gaseous Fuel
10.5-105 GJ/h	49.6 ppm
>105 GJ/h	76.3 ppm

If the emissions from your process are not from a boiler or heater within this capacity range, then limits for how much NO<sub>x</sub> can be emitted are taken from O. Reg. 419/05: Air pollution- local air quality [54]. For nitrogen oxides, the amount is calculated by using the following formula:

$$A = (B \times 1.53) + C \quad (8)$$

Where “A” is the amount (or concentration) of nitrogen oxides, “B” is the amount (or concentration) of nitric oxide, and “C” is the amount (or concentration) of nitrogen dioxide. The limit for nitrogen oxides is 500  $\mu\text{g}/\text{m}^3$  produced during half an hour [54].

#### 2.4.4 CO<sub>2</sub> emissions standards and regulatory context

While ammonia decomposition itself does not produce CO<sub>2</sub>, it requires electricity, making the emissions associated with the process dependent on the energy source. This model assumes that electricity is sourced from the Ontario electricity grid. Table 2.5 provides a breakdown of Ontario’s electricity generation sources. Since the grid is not entirely renewable, a portion of the electricity used results in CO<sub>2</sub> emissions. In 2025, Ontario's electricity emissions intensity is forecasted at 29 gCO<sub>2e</sub>/kWh, increasing to 64 gCO<sub>2e</sub>/kWh in 2027 before declining to 10 gCO<sub>2e</sub>/kWh by 2042, assuming advancements in renewable energy adoption and new technologies. These values will vary depending on location and changes in energy infrastructure [55].

Table 2.5: Ontario's electricity source [55].

Percentage (%)	Source
12.65	Natural Gas
0	Coal
53.27	Nuclear
25.13	Hydroelectricity
8.21	Wind
0.49	Solar
0.23	Bioenergy

The amount of carbon dioxide in this process is calculated by:

$$CO_2 \text{ emissions } \left( \frac{gCO_2e}{kg H_2} \right) = \text{total electricity consumption } \left( \frac{kWh}{kg H_2} \right) * \text{Ontario's electricity emissions } \left( \frac{gCO_2e}{kWh} \right) \quad (9)$$

## 2.4 Existing models and simulations

Large-scale ammonia cracking, especially for refuelling station applications, has been less extensively studied than ammonia synthesis. However, several recent techno-economic analyses and process simulations have helped advance the understanding of its feasibility and design. One key study by Nasharuddin et al. [33] evaluated the use of ammonia as a hydrogen carrier for fuel cell vehicle applications. Using Aspen HYSYS, they simulated two scales of operation: a centralized plant producing 1000 tons of hydrogen per day, and a distributed refuelling station producing 500 kg/day. The study concluded that centralized production is technically and economically viable, with a minimum hydrogen cost of USD\$5.50/kg, while distributed production was not economically favourable. They found that hydrogen cost is highly sensitive to ammonia feedstock prices, with moderate sensitivity to utility costs.

A more recent study by Devkota et al. [50] (2024) explored a different configuration: a catalytic packed-bed reactor with intermediate heating for ammonia decomposition. Their model incorporated both process and economic parameters, including furnace temperature, flue gas recirculation, system pressures, hydrogen purification, and equivalence ratio. The simulation achieved a thermal efficiency of 79% and produced 514 kg/h of 99.99% pure hydrogen from 4000 kg/h of ammonia. The levelized cost of hydrogen (LCOH) was USD\$6.05/kg, with ammonia feedstock accounting for over 60% of that cost. With a 25-year plant life and 10% discount rate, the design showed a 23.7% return on investment and a 3.58-year payback period.

Finally, Lee et al. [19] assessed a small-scale, on-site hydrogen refuelling station with a production capacity of 30 m<sup>3</sup>/h in Korea. Their techno-economic simulation estimated a hydrogen selling price of USD\$9.06/kg, with capital and operating costs totalling USD\$6.27/kg. Financial metrics, including a net present value of USD\$318,666, a discounted payback period of 2.24 years, and a present value ratio of 3.35, confirmed the economic feasibility of small-scale ammonia-to-hydrogen systems for local refuelling.

While all of these studies provide valuable insights into the techno-economic feasibility of ammonia cracking for hydrogen production, they rely heavily on commercial process simulation tools such as Aspen HYSYS, which can be costly and inaccessible to smaller research teams or public institutions.

In contrast, this study explores the ammonia decomposition process using open-source modelling tools, making the analysis more transparent, adaptable, and accessible. Additionally, in the literature, there are no studies examining this process specifically in Ontario or Canada, where factors such as local energy prices, regulatory frameworks, and refuelling infrastructure could significantly impact feasibility. This research aims to fill that gap by modelling a representative ammonia-to-hydrogen system tailored to Ontario using open tools and region-specific assumptions.

# Chapter 3 Methodology

## 3.1 Process Description

To produce hydrogen from ammonia, there are several key components. Figure 3.1 shows the process flow diagram of the ammonia decomposition process. The process begins with ammonia being fed from a storage tank to a pump. The ammonia is typically stored at cryogenic temperatures and ambient pressure. The pump is used to pressurize ammonia to the operating pressure of the reactor. However, before entering the reactor, the liquid ammonia must be vaporized and preheated to the operating temperature of the reactor. This is achieved using heat exchangers and furnaces. The core of the system is the reactor, where ammonia is decomposed into hydrogen and nitrogen. As discussed earlier, this can be a packed bed reactor or a membrane reactor. Since ammonia decomposition is an endothermic reaction, a continuous external heat source is required to maintain the reactor's operating temperature, which typically ranges between 400°C and 800°C. Depending on the reactor type, a hydrogen purification system may follow. For example, PBRs usually require a pressure swing adsorption (PSA) column to separate hydrogen from other gases, while MRs integrate a hydrogen-selective membrane to achieve high purity and recovery. Once separated, the hydrogen stream often passes through a cooling system. If a heat exchanger is used here, it can also help recover thermal energy to preheat incoming ammonia or power auxiliary systems, improving overall efficiency. Meanwhile, the unconverted ammonia and unrecovered hydrogen from the retentate side of the membrane will be fed into the furnace to produce heat. Throughout the process, control systems and sensors are critical for monitoring temperature, pressure, and flow rates. It's also important to measure hydrogen purity, as membrane leaks or process impurities can affect fuel cell performance. Finally, robust safety systems, including pressure relief valves, ammonia leak detectors, purge systems, and emergency shutdown protocols, must be in place to ensure safe and reliable operation of the ammonia cracking unit.

For this thesis, a packed bed membrane reactor was chosen since it combines the reaction and separation in one unit, reducing the need for downstream separation processes. Electric heater is used for to provide heat for ammonia decomposition in the PBMR to decarbonize industry heat. Part of the ammonia feedstock will combine with the retentate outlet stream in PBMR in the furnace to preheat the inlet stream to reduce electricity consumption.

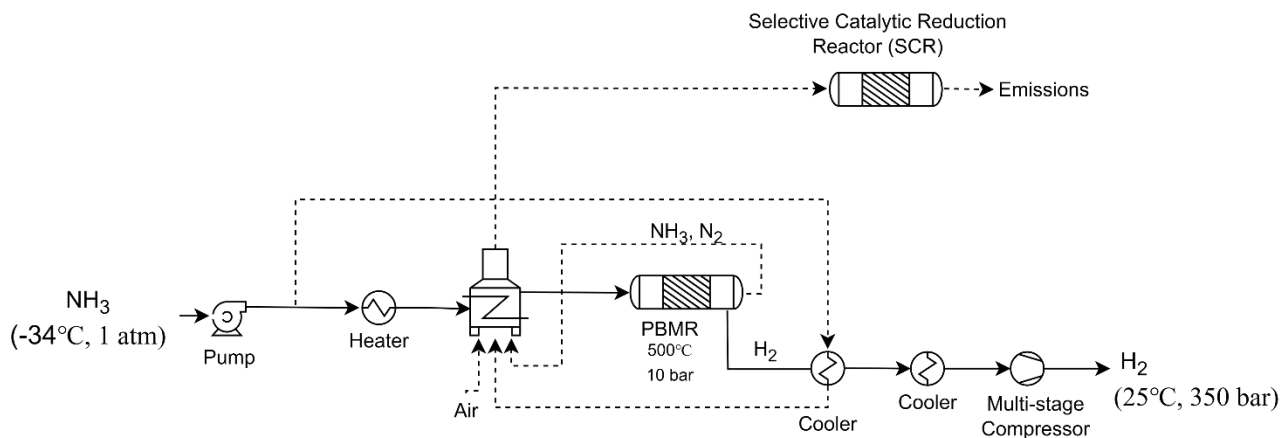


Figure 3.1: Ammonia decomposition process flow diagram with MR.

## 3.2 Model Development

### 3.2.1 Software and computational tools

All modelling and simulation work was done using Python, an open-source programming language widely used in scientific computing and engineering. Python is a powerful tool for chemical process modelling as it offers extensive libraries for numerical analysis, data handling, and visualization. Python facilitated the integration of multiple simulation components in a single environment, including chemical kinetics, thermodynamic calculations, and differential equation solving. In this thesis, Cantera [56] was used to calculate thermodynamic properties, evaluate chemical reaction rates based on kinetic mechanisms, determine transport properties and handle equilibrium calculations. Cantera is an open-source chemical kinetics and thermodynamics library that supports the simulation of chemically reacting flows that can be used in Python. Cantera provides access to robust, internally consistent property data and supports the integration of custom reaction mechanisms. Another important library that was used in Python was scikits.odes [57] that was used to solve differential-algebraic equations (DAEs). This is a Python wrapper for the SUNDIALS suite of solvers, such as CVODE and IDA. This library was selected to solve DAE as it can handle stiff systems, common in chemical reacting systems with fast and slow dynamics. It also efficiently solves coupled systems of ordinary differential equations and algebraic constants.

### 3.2.2 Governing Equations

#### 3.2.2.1 Reactor

The packed bed membrane reactor was modelled based on a model from Kogekar [36]. The main assumptions for this model were that the reactor operated at steady-state and flow is one-dimensional.

To model the reactor, the following equations were used which are the mass continuity, gas phase species continuity and energy. Where  $k$  is the chemical species (ammonia, hydrogen, nitrogen etc,) and  $K_g$  is the number of chemical species in the gas phase.

$$\frac{d(\rho u)}{dz} = A_s \sum_{k=1}^{K_g} \dot{s}_k W_k - \frac{P_b}{A_b} j_{k_M} \quad (10)$$

$$\rho u \frac{d(Y_k)}{dz} + A_s Y_k \sum_{k=1}^{K_g} \dot{s}_k W_k = (\phi_g \dot{w}_k + A_s \dot{s}_k) W_k - \delta_{k,k_M} \frac{P_b}{A_b} j_{k_M}, \quad (k = 1, \dots, K_g) \quad (11)$$

$$\rho u c_p \frac{dT}{dz} + \sum_{k=1}^{K_g} h_k [(\phi_g \dot{w}_k + A_s \dot{s}_k) W_k] = \hat{h} \frac{P_b}{A_b} (T_w - T) - \delta_{k,k_M} \frac{P_b}{A_b} h_{k_M} j_{k_M} \quad (12)$$

In this model, the conservation of surface species was also taken into consideration. As the model is considered to be in steady state (the surface coverage does not vary with time), the net production of surface species is zero.

$$\dot{s}_k = 0 \quad (13)$$

Other equations (14-16) that are taken into consideration for this model are the pressure drop and the membrane flux.

$$\frac{d_p}{dz} = - \left( \frac{\phi_g \mu}{\beta_g} \right) u \quad (14)$$

$$\beta_g = \frac{\phi_g^3 D_p^2}{72 \tau_g (1 - \phi_g)^2} \quad (15)$$

$$j_{k_M}^{Mem} = \frac{B_{k_M}}{t_m} (\mathcal{P}_{k_M,mem}^\alpha - \mathcal{P}_{k_M,sweep}^\alpha) W_{k_M}, \quad \text{where } \alpha = 1 \quad (16)$$

Constraints that need to be taken into consideration for this model are that the summation of the species coverages and mass fractions are both equal to 1. This is described in the two equations (17) below.

$$\sum_{k=1}^{K_s} \theta_k = 1 \quad \text{and} \quad \sum_{k=1}^{K_g} Y_k = 1 \quad (17)$$

In addition, for this model, a 12-step surface reaction mechanism based on a nickel catalyst was used. The specific type of catalyst used was Ni BCZYYb ( $\text{BaCe}_{0.7}\text{Zr}_{0.1}\text{Y}_{0.1}\text{Yb}_{0.1}\text{O}_{3-\delta}$ ) [58] which has a density of  $2.6079 \times 10^{-9} \text{ mol/cm}^2$  and the mechanism can be found in Table 3.1.

Table 3.1: Catalyst mechanism Ni-BCZYYB [58].

Reaction	A (cm, s)	b	Ea (kJ/mol)
1. $N_2 + Ni(s) + Ni(s) \rightarrow N(s) + N(s)$ (Sticking coefficient)	$1.378 * 10^{-6}$	0.000	47.88
2. $N(s) + N(s) \rightarrow Ni(s) + Ni(s) + N_2$	$2.168 * 10^{16}$	-0.126	120.2
3. $H_2 + Ni(s) + Ni(s) \rightarrow H(s) + H(s)$ (Sticking coefficient)	$1.973 * 10^{-3}$	0.000	0.000
4. $H(s) + H(s) \rightarrow Ni(s) + Ni(s) + H_2$	$5.655 * 10^{20}$	-0.117	111.5
5. $NH_3 + Ni(s) \rightarrow NH_3(s)$ (Sticking coefficient)	$1.900 * 10^{-5}$	-0.097	0.020
6. $NH_3(s) \rightarrow Ni(s) + NH_3$	$5.791 * 10^{11}$	-0.161	80.64
7. $H(s) + N(s) \rightarrow NH(s) + Ni(s)$	$7.000 * 10^{20}$	-0.161	84.40
8. $NH(s) + Ni(s) \rightarrow H(s) + N(s)$	$6.177 * 10^{19}$	0.161	29.98
9. $NH(s) + H(s) \rightarrow NH_2(s) + Ni(s)$	$7.724 * 10^{19}$	-0.161	76.48
10. $NH_2(s) + Ni(s) \rightarrow NH(s) + H(s)$	$5.332 * 10^{19}$	0.161	14.53
11. $NH_2(s) + H(s) \rightarrow NH_3(s) + Ni(s)$	$6.062 * 10^{19}$	-0.161	22.28
12. $NH_3(s) + Ni(s) \rightarrow NH_2(s) + H(s)$	$1.780 * 10^{20}$	0.161	60.20

For evaluating the surface kinetics, either the sticking coefficient or the Arrhenius equation was used. Surface reactions are often described in terms of the sticking coefficient as well as coverage dependencies. Only reactions 1,3, and 5 use the sticking coefficient, while the rest of the mechanism reactions use the Arrhenius equation to calculate the rate constant. The sticking coefficient may be

represented in terms of collision frequency in equation 18. While the forward rate expression can be evaluated as seen in equation 19.

Sticking Coefficient [59]:

$$\gamma_i = aT^b \exp\left(\frac{Ea}{RT}\right) \quad (18)$$

$$k'_i = \frac{\gamma_i}{\Gamma^m} \sqrt{\frac{RT}{2\pi W_k}} \quad (19)$$

$$k_i = k'_i \prod_{k=1}^K \exp\left(-\frac{\varepsilon_{k,i}\theta_k}{RT}\right) \quad (20)$$

Arrhenius equation [59]:

$$k_i = AT^b \exp\left(-\frac{Ea}{RT}\right) \quad (21)$$

### 3.2.2.2 Pump

As mentioned previously, ammonia can be stored as a liquid at approximately -34°C and 1 atm. However, typically the operating pressure of ammonia decomposition is higher than 1 atm. Since the pressure needs to be increased and ammonia is a liquid in these conditions, a cryogenic pump is required. A cryogenic pump is a type of pump that is designed to handle extremely low-temperature fluids, which include liquid ammonia. Even with needing a cryogenic pump, which may require additional handling to prevent heat transfer and phase change, general equations for calculating actual work will be used.

The first law of thermodynamics states that energy cannot be created or destroyed, but it can change forms. With assumptions such as the operation is at steady state, the process is adiabatic and reversible (isentropic), isentropic efficiency of around 70%, and the change in potential and kinetic energy is negligible (or ignored), the energy balance for the first law of thermodynamics is [23]:

$$Work = Enthalpy_{in} - Enthalpy_{out} \quad (22)$$

### 3.2.2.3 Heat exchangers

To model the heat exchangers, the assumptions were that the process is at steady state, adiabatic, counter-current flow, and no pressure drop. From this, the following equations were used.

Pre-phase change (sensible heating of liquid)

$$Q_{pre} = \dot{m}_c \times C_{p,liquid} \times (T_{phase\ change} - T_{in,c}) \quad (23)$$

Phase change (latent heat of vaporization)

$$Q_{phase} = \dot{m}_c \times h_{latent} \quad (24)$$

Post-phase change (sensible heating of gas)

$$Q_{post} = \dot{m}_c \times C_{p,vapor} \times (T_{out,c} - T_{phase\ change}) \quad (25)$$

Then all the heats are summed together.

$$Q_{total} = Q_{pre} + Q_{phase} + Q_{post} \quad (25)$$

In addition, since the cost will be calculated, finding the area of the heat exchanger is important; therefore, the log mean temperature difference was calculated.

$$T_{out,h} = T_{in,h} - \frac{Q_{total}}{\dot{m}_h \times C_{p,h}} \quad (26)$$

$$\Delta T_1 = T_{in,h} - T_{out,c} \quad (27)$$

$$\Delta T_2 = T_{out,h} - T_{in,c} \quad (28)$$

$$\Delta T_{lm} = \frac{\Delta T_1 - \Delta T_2}{\ln\left(\frac{\Delta T_1}{\Delta T_2}\right)} \quad (29)$$

Using the log mean temperature difference, the area can be calculated.

$$A = \frac{Q_{total}}{U_{HX} \times \Delta T_{lm}} \quad (30)$$

For the second, third and fourth heat exchangers, since there is no phase change, the only heat calculated was for the sensible heat of a gas.

### 3.2.2.4 Ammonia combustion and SCR

To heat the ammonia entering the reactor, a heater or furnace is required. Therefore, a portion of ammonia is combusted to produce this heat. To simulate ammonia combustion, the Cantera function “equilibrate” was used. This function determines the chemical equilibrium composition of a mixture by minimizing the total Gibbs free energy of the system, subject to other constraints such as constant pressure or enthalpy. In this study, the reactor was assumed to operate under adiabatic and steady-state conditions, meaning no heat was exchanged with the surroundings. Under this assumption, the combustion process was simulated using constant enthalpy and pressure, which yields the adiabatic temperature and corresponding equilibrium composition.

The chemical equilibrium is found by minimizing the system's total Gibbs free energy, which can be calculated using equations 31-32 [60].

$$\min G(T, P, n_i^\pi) = \sum_{i=1}^{NC} \sum_{\pi=1}^{NP} n_i^\pi \cdot \mu_i^\pi \quad (31)$$

$$s. t.: n_i^\pi \geq 0$$

$$\sum_{\pi=1}^{NF} n_i^\pi = n_i^0 + \sum_{j=1}^{NR} v_{ij} \xi_j \quad (32)$$

Where  $n_i^\pi$  and  $\mu_i^\pi$  are the number of moles and chemical potential, respectively, for each  $i$  component of each  $\pi$  phase.  $n_i^0$  is the initial number of moles of each  $i$  component,  $v_{ij}$  is the stoichiometric coefficient of the  $i$  component in the  $j$  reactions, and  $\xi_j$  is the extent of the reaction  $j$  for the number of independent reactions (NR).

Although the equilibrium model does not account for reaction kinetics or residence time effects, it provides insight into thermodynamically feasible NO<sub>x</sub> emissions during ammonia combustion. At the elevated temperatures predicted under adiabatic conditions, significant formation of NO and NO<sub>2</sub> may occur due to the partial oxidation of ammonia and thermal dissociation reactions involving nitrogen species. To address this, a Selective Catalytic Reduction (SCR) unit is included downstream of the combustor to reduce NO<sub>x</sub> emissions. To simplify integration within the simulation, the SCR system is represented as a black-box model. A fixed NO<sub>x</sub> conversion efficiency of 85% is assumed, and the output gas composition is adjusted accordingly to reflect reduced NO and NO<sub>2</sub> concentrations. The energy impact of the SCR unit is incorporated through an enthalpy balance, under the assumption that the unit operates under isenthalpic conditions or with minimal heat exchange. The total enthalpy of the outlet stream is computed based on the post-conversion gas composition and temperature, ensuring consistency with the first law of thermodynamics.

### 3.2.2.5 Multi-stage hydrogen compressor

Hydrogen is being used in an on-site fueling station; therefore, the pressure needs to be increased to 350 bar. For the compressor, the isentropic method was assumed where the process is adiabatic. The isentropic efficiency was assumed to be 72%.

From literature, Franco et al.[12] used the following equations to calculate the isentropic work of the compressor with different numbers of stages.

$$w_{is} = N * \left(\frac{k}{k-1}\right) \left(\frac{Z}{\eta_{is}}\right) * R * T_{in} \left[\left(\frac{P_{st}}{P_{in}}\right)^{\frac{k-1}{Nk}} - 1\right] \quad (33)$$

Another way this can be written is with enthalpy. Let's take an example with four stages.

$$w_{is} = \frac{(h_{2is} - h_1) + (h_{4is} - h_3) + (h_{6is} - h_5) + (h_{8is} - h_7)}{\eta_{is}} \quad (34)$$

Once the specific work per unit mass is calculated using either equation 33 or 34, the total power input can be found using:

$$P = \dot{m} * w_{is} \quad (35)$$

To distribute the pressure evenly across N stages, the intermediate pressure for each stage must be calculated. This ensures each stage compresses the same pressure ratio:

$$\beta = \left(\frac{P_{st}}{P_{in}}\right)^{\frac{1}{N}} \quad (36)$$

Then, the pressure after the  $i^{\text{th}}$  stage is:

$$P_{int,i} = P_{in} \beta^i \text{ with } i = 1, 2, \dots, (N - 1) \quad (37)$$

This defines the outlet pressure of each intermediate stage, which is also the inlet pressure for the next. For hydrogen compressors, the compression ratio cannot exceed 7, and ideally, the maximum temperature during compression should not exceed 150-200°C [12].

## 3.3 Model set up and validation

### 3.3.1 Reactor Validation

First, the reactor was modelled at a small scale to compare with the study done by Kogekar [36]. Table 3.2 presents the parameters used for comparing the results of a packed bed reactor with and without a membrane.

Table 3.2: Small-scale ammonia decomposition reactor parameters.

Parameters	Value
Length (m)	7.0e-2
Radius (m)	5.0e-3
$\phi_g$	0.6
$\tau_g$	2.0
$d_p$ (m)	3.4e-4
$A_s$ (1/m)	9.7e6
$B_{k_M} \left( \frac{\text{kmol} * \text{m}^3}{\text{s} * \text{Pa}} \right)$	5.7e-15
t (m)	3.0e-6
$P_{in}$ (Pa)	5.0e5
$v_{in}$ (m/s)	0.03
$T_w$ (K)	723
$\hat{h} \left( \frac{\text{W}}{\text{m}^2 * \text{K}} \right)$	1.0e2
$y_{NH_3in}$	0.99
$y_{Arin}$	0.01
$\mathcal{P}_{k_M, sweep}^\alpha$ (Pa)	1.0e4
$T_{in}$ (K)	723

Figure 3.2 illustrates a consistent trend across all three datasets, which are experimental results from the referenced paper, the paper’s model predictions, and the results from this model. All datasets show a decreasing trend in ammonia conversion as the gas hourly space velocity (GHSV) increases. This behaviour is expected because higher GHSV corresponds to a shorter residence time for ammonia in the reactor, which limits the extent of the reaction and reduces the conversion efficiency. A closer comparison of the results reveals that this model’s predictions align more closely with the paper’s model results than with the experimental data. This could be attributed to the modelling assumptions, particularly the use of one-dimensional flow in the simulations, which may introduce simplifications

that bring the two sets of model results into closer agreement. Additionally, it is evident from the figures that as the temperature decreases, the ammonia conversion for all GHSV values also declines. This observation highlights the temperature-dependent nature of ammonia decomposition, as the reaction is thermodynamically and kinetically favoured at higher temperatures. It can be concluded that ammonia decomposition achieves significantly better performance under high-temperature conditions, reinforcing the importance of maintaining elevated operating temperatures to maximize conversion efficiency.

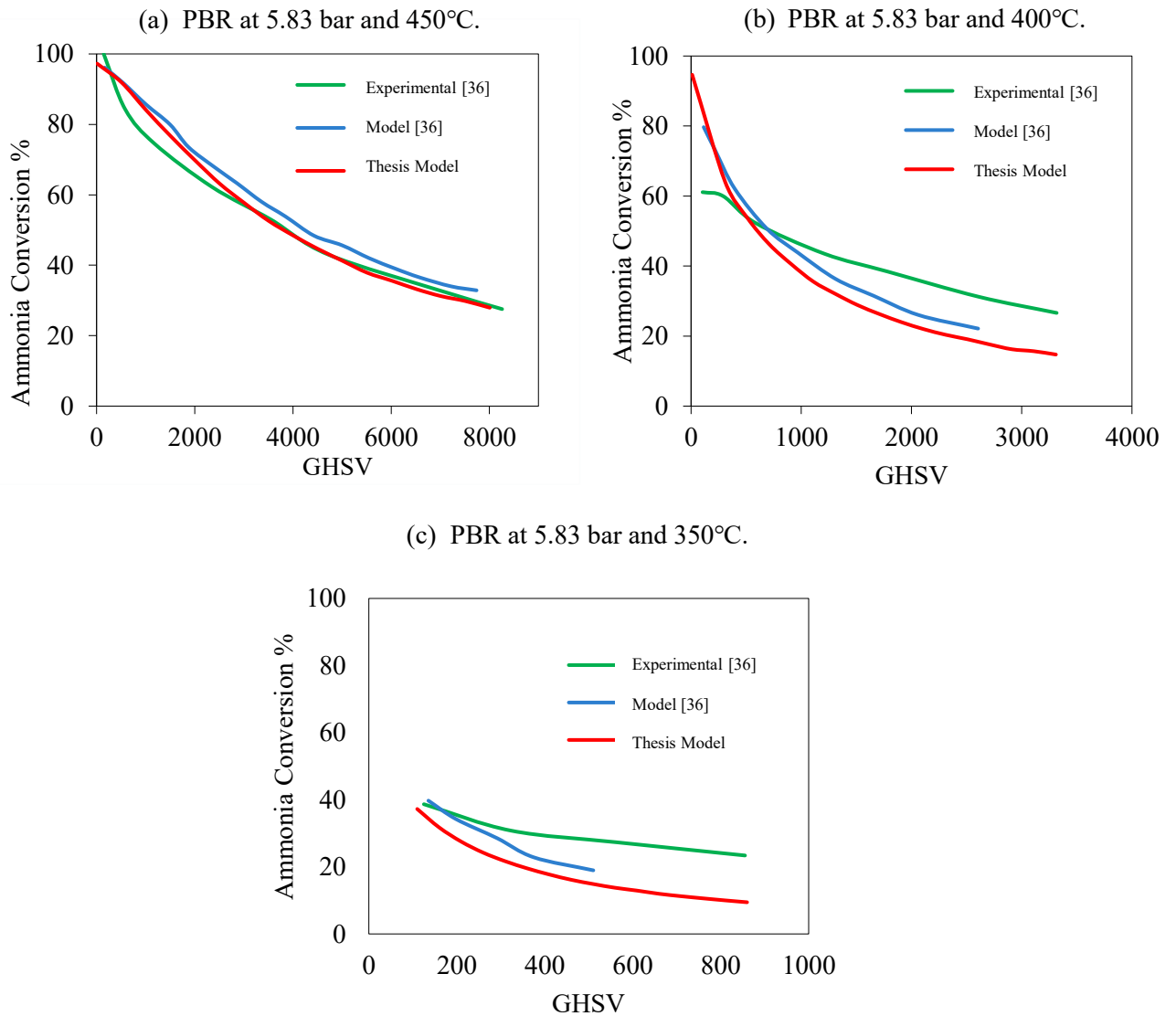


Figure 3.2: Small-scale PBR results from Kogekar [36] vs current model.

In Figure 3.3 (a), the ammonia mole fraction decreases progressively along the reactor length, as expected. This trend reflects the continuous decomposition of ammonia as it moves through the reactor. In Figure (b) and (c), the mole fraction of hydrogen and nitrogen, respectively, increases

along the reactor length. This increase is consistent with the stoichiometric decomposition of ammonia, where ammonia breaks down into hydrogen and nitrogen. In Figure 3.3, the hydrogen mole fraction is significantly lower in the PBMR compared to the PBR. This is because, in the PBMR, hydrogen is selectively separated from the reactor through a palladium (Pd) membrane. This separation results in lower hydrogen mole fractions within the reactor but facilitates the recovery of high-purity hydrogen outside the reaction zone. Across all three figures, the results from the model closely align with the experimental data provided in the literature for both reactor configurations. This agreement validates the accuracy and robustness of the model in capturing the key dynamics of ammonia decomposition for both PBR and PBMR designs. These results also highlight the distinct operational characteristics of each reactor type and emphasize selective product separation for PBMR.

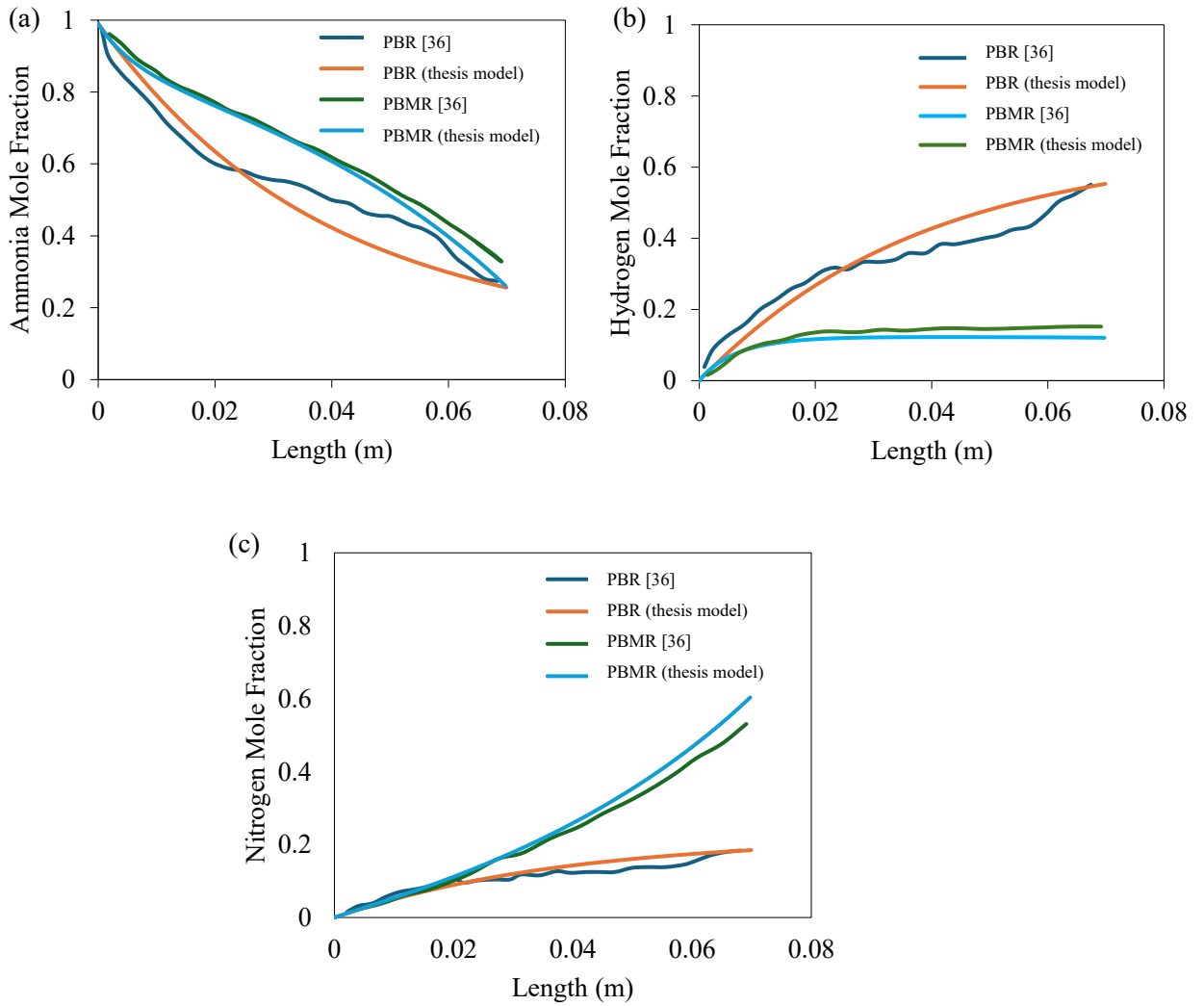


Figure 3.3: Packed bed reactor with and without membrane Kogekar [36] vs current model.

In this reaction, several surface species are involved, but the analysis focuses on three key intermediates: N(s), H(s), and Ni(s). The surface coverages of these species were examined along the reactor length for PBR. In the PBR, surface coverages vary significantly along the reactor length. The continuous flow of ammonia, combined with the depletion of reactants and the accumulation of products, generates pronounced gradients in surface coverage. Figure 3.4 shows the species coverage over the length of the reactor for the model and from the paper by Kogekar [36].

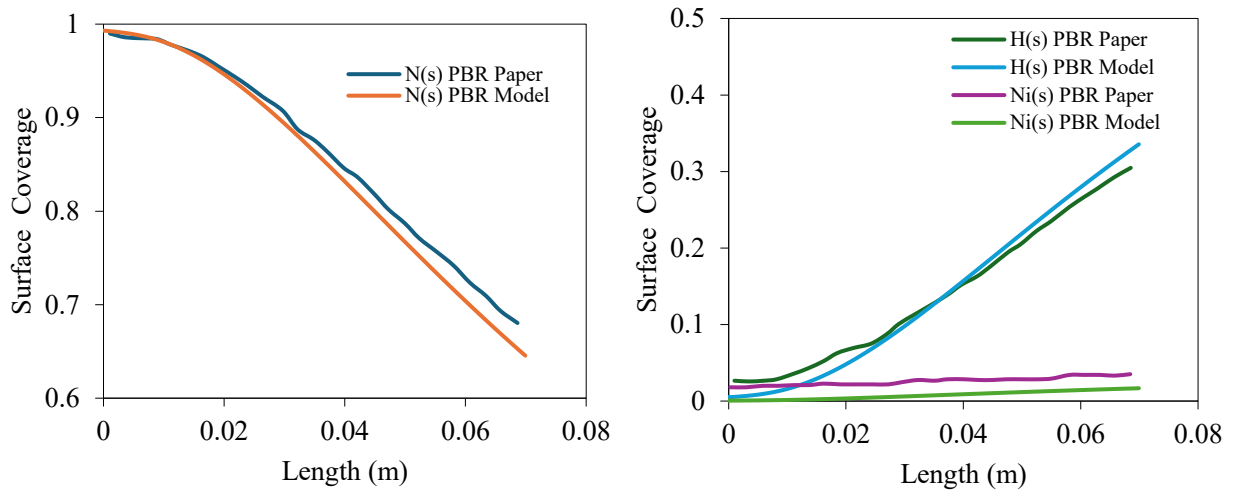


Figure 3.4: PBR species coverage (300 SCCM, 5 bar, 450°C).

# Chapter 4 Base Case Results

## 4.1 Reactor Results

The previous section thoroughly validated the reactor model against literature data, demonstrating its accuracy and reliability in predicting reactor performance under a range of conditions. Building on this foundation, this section will focus on the next crucial step: scaling up the reactor. The goal is to transition from small-scale to designing a reactor capable of meeting larger-scale hydrogen production demands, while maintaining efficiency, minimizing emissions, and ensuring economic feasibility.

To scale up, it is essential to determine the station's capacity. It is important to note that this refuelling station will be catering to heavy-duty vehicles. Assuming that each heavy-duty truck has a hydrogen consumption rate of 9.04 kg/100km and can travel approximately 500km before refuelling, then each HDT would need 45.2kg of hydrogen. This station will provide 500kg of hydrogen per day. Therefore, this station will service 11 trucks per day [20].

Once the capacity of the refuelling station was determined, the reactor length was increased to 1.6m. A packed-bed membrane reactor configuration was selected due to its simultaneous reaction separation capability. The reactor operates under steady-state conditions, with the retentate stream flowing through the inside of the membrane tube and the permeate stream on the outside. A co-current flow configuration is employed within a packed-bed membrane reactor. The design parameters and operating conditions used for modelling a large-scale reactor are summarized in Table 4.1.

Table 4.1: Large-scale ammonia decomposition membrane reactor parameters.

Parameters	Value
Length (m)	1.6
Radius (m)	0.5
$\phi_g$	0.6 [11]
$\tau_g$	2 [11]
$d_p$ (m)	3.4e-4 [11]
$\rho_{k_M, sweep}^\alpha$ (Pa)	1.0e5 [7]
$T_{in}$ (K)	773 [22]
$P_{in}$ (bar)	10 [22]
$A_s$ (1/m)	9.7e6 [11]
Permeance ( $\frac{\text{kmol}}{\text{s} * \text{m}^2 * \text{Pa}}$ )	2.3e-9 [39]

With the reactor configuration and dimensions defined, the next step was to evaluate whether the reactor should operate isothermally or adiabatically. This began by first plotting and examining the temperature profile along the length of the reactor.

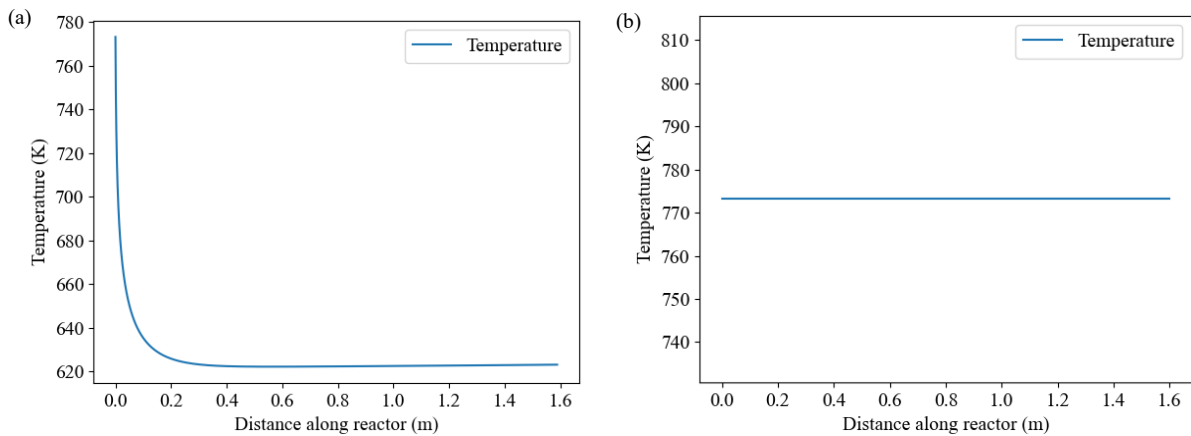


Figure 4.1: Temperature profile along the length of the reactor under (a) adiabatic and (b) isothermal conditions.

Then, after plotting the temperature profiles, the flow rates were plotted.

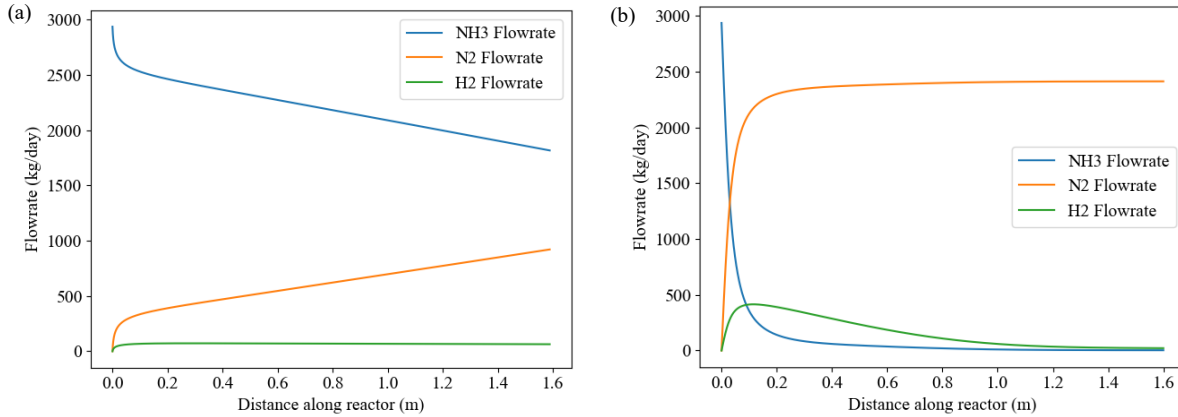


Figure 4.2: Flow rate along the length of the reactor under (a) adiabatic and (b) isothermal conditions.

As seen in Figure 4.1 (a), the temperature drops from 773 K to 623K when operating adiabatically. Due to the temperature drop, the ammonia conversion rate reaches only 38% when the reactor is set to a length of 1.6m. This can be seen in Figure 4.2 (a), where it shows there is still a considerable amount of ammonia in the retentate stream. When comparing to Figure 4.1(b), where the reactor is operating isothermally (constant temperature of 773K), the ammonia conversion is almost complete at 99.92%. This can be seen in Figure 4.2 (a), where there is hardly any ammonia left and it is all converted to nitrogen and hydrogen. Since the reaction is endothermic, operating under adiabatic conditions results in a continuous temperature drop along the reactor length due to heat consumption by the reaction. However, under isothermal conditions, the heat was maintained, allowing for the reaction to proceed as the reaction favours higher temperatures. From this, an isothermal approach was selected over adiabatic operation. This decision was made to maintain a higher and more consistent conversion rate of ammonia to hydrogen.

Expanding on Figure 4.2(b) as the chosen mode of thermal operation, the flow rate of ammonia decreases progressively as it decomposes into hydrogen and nitrogen through the catalytic reaction. The decomposition rate is highest near the reactor inlet due to the high concentration of ammonia. It gradually slows down along the reactor length as the reactant concentration decreases and the reaction rate drops. Simultaneously, the hydrogen concentration increases along the reactor; however, due to the presence of a selective membrane, hydrogen is continuously removed from the retentate side, resulting in a slower accumulation than would be observed in a non-membrane system. Nitrogen, like hydrogen, starts at zero and increases steadily along the reactor length as a product of the decomposition reaction. Figure 4.3 shows the flow rate on the retentate side, which consists mainly of

nitrogen and small amounts of unconverted ammonia and hydrogen that did not permeate through the membrane.

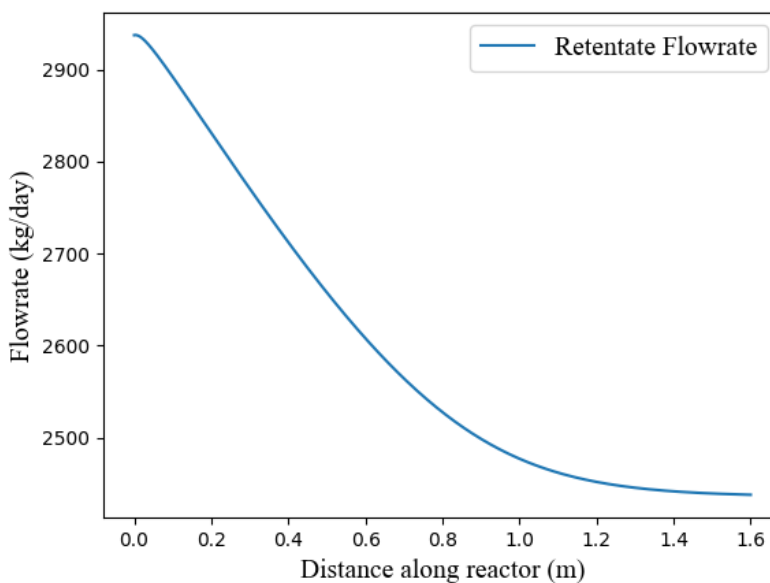


Figure 4.3: Ammonia decomposition reactor overall retentate flowrate.

Figure 4.4 provides further insight into the surface reaction mechanism by showing the site fraction profiles of adsorbed species on the catalyst surface, including Ni(s), N(s), H(s), NH(s), NH<sub>2</sub>(s), and NH<sub>3</sub>(s). These surface species play a crucial role in the stepwise decomposition of ammonia. Initially, NH<sub>3</sub> is adsorbed onto the nickel catalyst surface, where it undergoes successive dehydrogenation steps to form NH<sub>2</sub>(s), NH(s), and eventually N(s) and H(s). The graphs reveal the coverage of each species along the reactor. The Ni(s) site fraction represents available active sites, which decrease near the inlet due to high surface coverage by adsorbed intermediates, then recover as species desorb or are consumed further along the reactor. These results highlight the importance of surface kinetics in controlling the overall reaction rate and provide a deeper understanding of the catalytic mechanism governing ammonia decomposition.

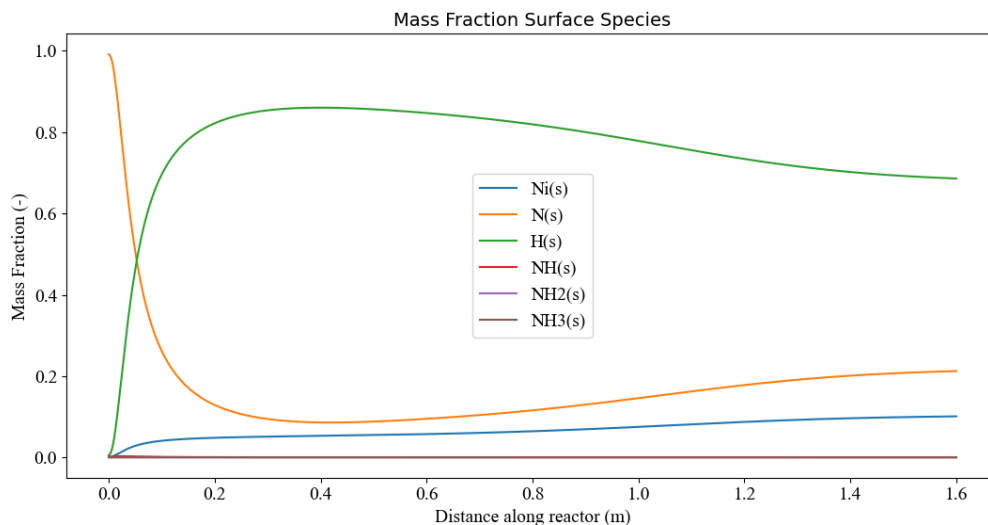


Figure 4.4: Ammonia decomposition reactor surface chemical species mass fraction.

Figure 4.5 shows the pressure profile along the length of the reactor. A continuous and gradual decrease in pressure is observed, starting from an initial value of 10 bar at the inlet and decreasing to approximately 9.99 bar at the outlet. This slight pressure drop is consistent with typical behaviour in packed bed reactors, where resistance to flow through the catalyst bed leads to a measurable loss in pressure due to friction and flow resistance. In reactor design, this pressure drop is generally expected and acceptable within certain limits. Monitoring and minimizing pressure drop are important aspects of reactor optimization to ensure reliable and efficient performance at an industrial scale.

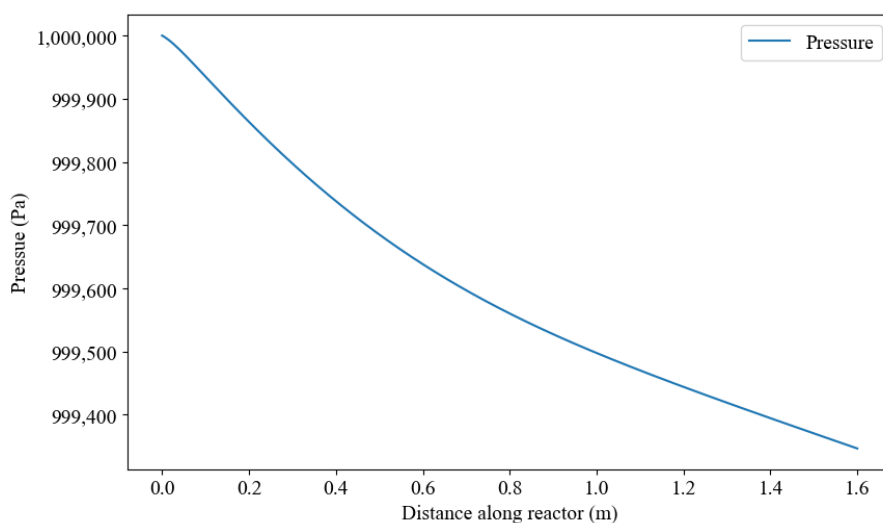


Figure 4.5: Pressure drop over the membrane reactor.

Table 4.2 provides a summary of the final operating conditions and output values at the reactor outlet. The reactor is maintained at a temperature of 773.15 K (500°C) to support high conversion rates for

the endothermic ammonia decomposition reaction. The final pressure at the reactor outlet is approximately 9.9935e5 Pa (9.99 bar), showing only a minor pressure drop from the inlet, consistent with expectations for flow through a packed bed.

The mass flow rates of the gas-phase species on the retentate side indicate the progress of the reaction and the effectiveness of the membrane separation. A small quantity of unconverted ammonia remains (2.4 kg/day), corresponding to a nearly complete ammonia conversion of 99.92%. This high conversion rate demonstrates the strong thermodynamic and kinetic driving forces supported by hydrogen removal through the membrane. The retentate stream is composed primarily of nitrogen (2414 kg/day), with a small fraction of hydrogen (21.2 kg/day) that was not removed by the membrane. The final mass fractions further confirm this composition: nitrogen dominates the retentate at 99.02%, with trace amounts of hydrogen (0.88%) and residual ammonia (0.1%).

The hydrogen recovery across the membrane is notably high at 95.9%, confirming that the membrane effectively separates hydrogen from the reaction zone. This selective removal plays a critical role in driving the equilibrium toward higher ammonia conversion while producing a permeate stream rich in hydrogen. The total mass flow rates indicate that the retentate contains 2438 kg/day, while the permeate stream, primarily hydrogen, accounts for 499.9 kg/day. These results demonstrate the feasibility of the membrane reactor design for large-scale ammonia cracking, achieving high conversion and efficient hydrogen recovery with small amounts of ammonia.

Table 4.2: Reactor summary of outlet stream.

<b>Parameter</b>	<b>Results</b>
Temperature (K)	773.15
Pressure (Pa)	9.9935e5
NH <sub>3</sub> Mass Flow (kg/day) Retentate	2.4057
H <sub>2</sub> Mass Flow (kg/day) Retentate	21.241
N <sub>2</sub> Mass Flow (kg/day) Retentate	2414.0
H <sub>2</sub> Mass Fraction Retentate (-)	0.0088
NH <sub>3</sub> Mass Fraction Retentate (-)	0.0010
N <sub>2</sub> Mass Fraction Retentate (-)	0.9902
NH <sub>3</sub> Conversion	0.9992
Total Mass Flow Retentate (kg/day)	2437.7
Total Mass Flow Permeate (kg/day)	499.9
H <sub>2</sub> Recovery (-)	0.9592

## 4.2 Process mass and energy balance

Figure 4.6 shows the ammonia decomposition process flow diagram, outlining how Python will solve this steady-state system. In the diagram, green streams represent air, red streams originate from the furnace outlet, and the blue stream corresponds to the portion of ammonia that is split, heated, and directed into the furnace.

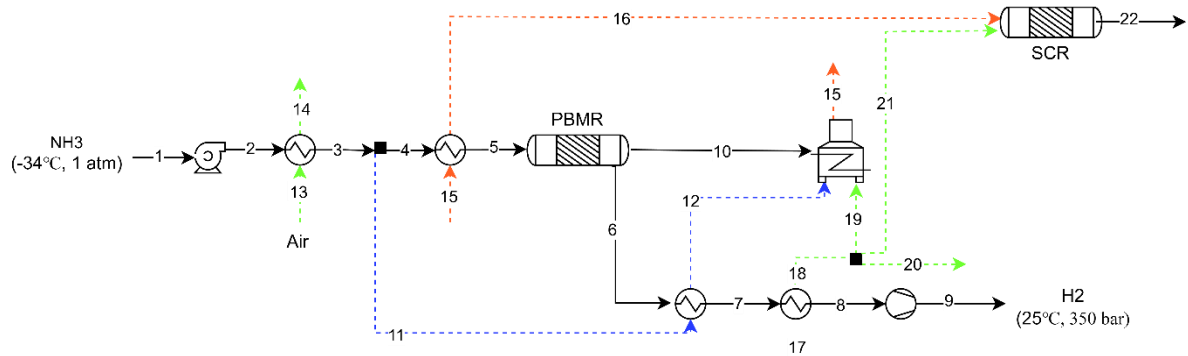


Figure 4.6: Process flow diagram for ammonia decomposition.

Figure 4.7 presents a flowchart detailing the computational process for solving the steady-state ammonia decomposition system. The process begins with defining all necessary input parameters required for the simulation. This includes values such as reactor temperature, all inlet streams and other values that are described in Table 4.3. Then in the code, a while loop is used to iteratively solve for the steady-state conditions of the system by updating compositions and energy balances until convergence is achieved. The key variables being iterated included the combustion, temperature and mass flow rate of the recycle stream (stream 15), as well as the mass flow rate of air needed for the furnace. The convergence was monitored using the mean squared error metric between successive iterations, and the loop was set to terminate once the mean squared error fell below a tolerance threshold of  $1e-5$ . To explain each step within the loop, liquid ammonia is pressurized by a cryogenic pump and then heated through two heat exchangers to reach  $500^{\circ}\text{C}$  before entering the reactor. In the reactor, ammonia decomposes into hydrogen and nitrogen, with hydrogen selectively removed via a membrane. The hydrogen stream is then cooled and compressed to 350 bar, while the residual on the retentate side of the membrane is combusted with some ammonia feedstock in a furnace to provide heat. An SCR unit removes  $\text{NO}_x$  emissions from the flue gas from the combustor. The process concludes by exporting the simulation results. The results for the base case for each stream and equipment, and compared to Aspen Plus, can be found in Appendix A Table A.1-A.6.

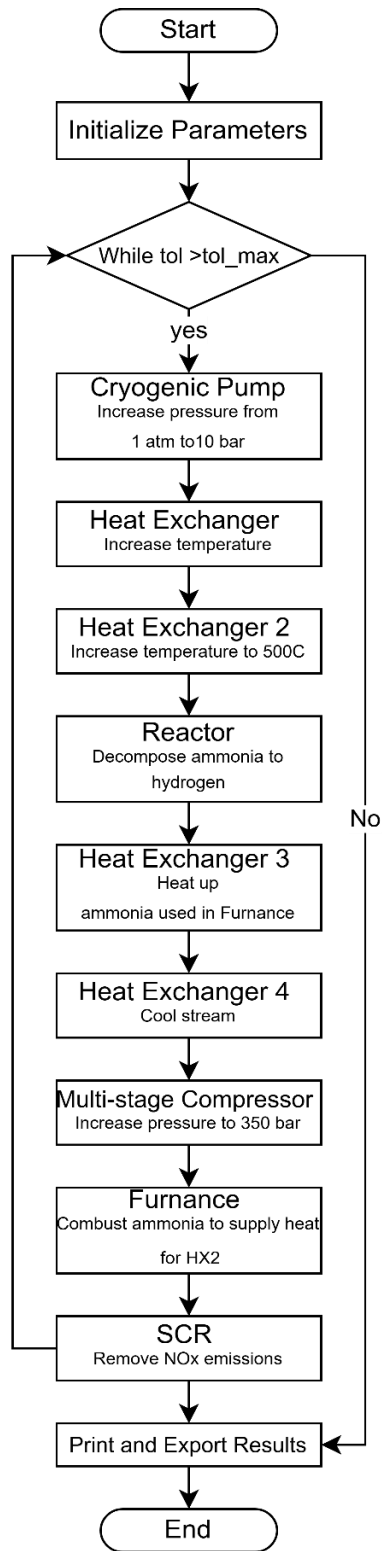


Figure 4.7: Process code diagram for ammonia decomposition.

Table 4.3: Summary of parameters used for the system.

Parameter	Results
Pump	
Isentropic efficiency	70%
Outlet Pressure	10bar
Heat Exchanger 1	
Cold temperature outlet	28°C
Heat Exchanger 2	
Cold temperature outlet	500°C
Heat Exchanger 3	
Cold temperature outlet	480°C
Heat Exchanger 4	
Cold temperature outlet	50°C
Multi-stage compressor	
Outlet pressure	350 bar
Isentropic Efficiency	72%
Number of Stages	5
Cooling temperature	180°C
Outlet temperature	25°C
Furnace	
Equivalence ratio	0.94
SCR	
NO <sub>x</sub> removal	85%

Figure 4.8 (a) shows a Sankey diagram representing the mass flow distribution in the ammonia decomposition process. Figure 4.8 (b) focuses on the bottom section of the Sankey diagram, excluding the air streams required for the heat exchangers, in order to visualize the distribution of the chemical species without the distortion caused by the relatively large air flow rates. The diagram tracks the primary inlet and outlet streams, with flow values in kg/day. Ambient air and ammonia are introduced as feed streams. A significant portion of the preheated air is ultimately discharged as air out, which comprises both the cyan stream (313,941 kg/day) and the purple stream (HX4 outlet, 3,802 kg/day) in Figure 4.8 (a), summing to a total air outlet of 317,743 kg/day. The ammonia feed enters the reactor, where catalytic decomposition occurs, producing hydrogen (500 kg/day). A portion of the

feed (179 kg/day) is diverted as fuel for the combustor, which supports the endothermic decomposition process. Combustion products (3,802 kg/day) flow into the SCR to control NO<sub>x</sub> emissions. The remaining flow from the reactor, including unreacted ammonia and byproducts, exits at 2,938 kg/day. This Sankey diagram highlights the flow of mass throughout the integrated ammonia cracking process. The widths of the flows represent the relative mass quantities, demonstrating that all major inlet and outlet streams are accounted for. This visualization supports the verification of mass conservation across the system, confirming that the mass of inputs is redistributed into hydrogen, nitrogen, and by-products, with no unexplained losses.

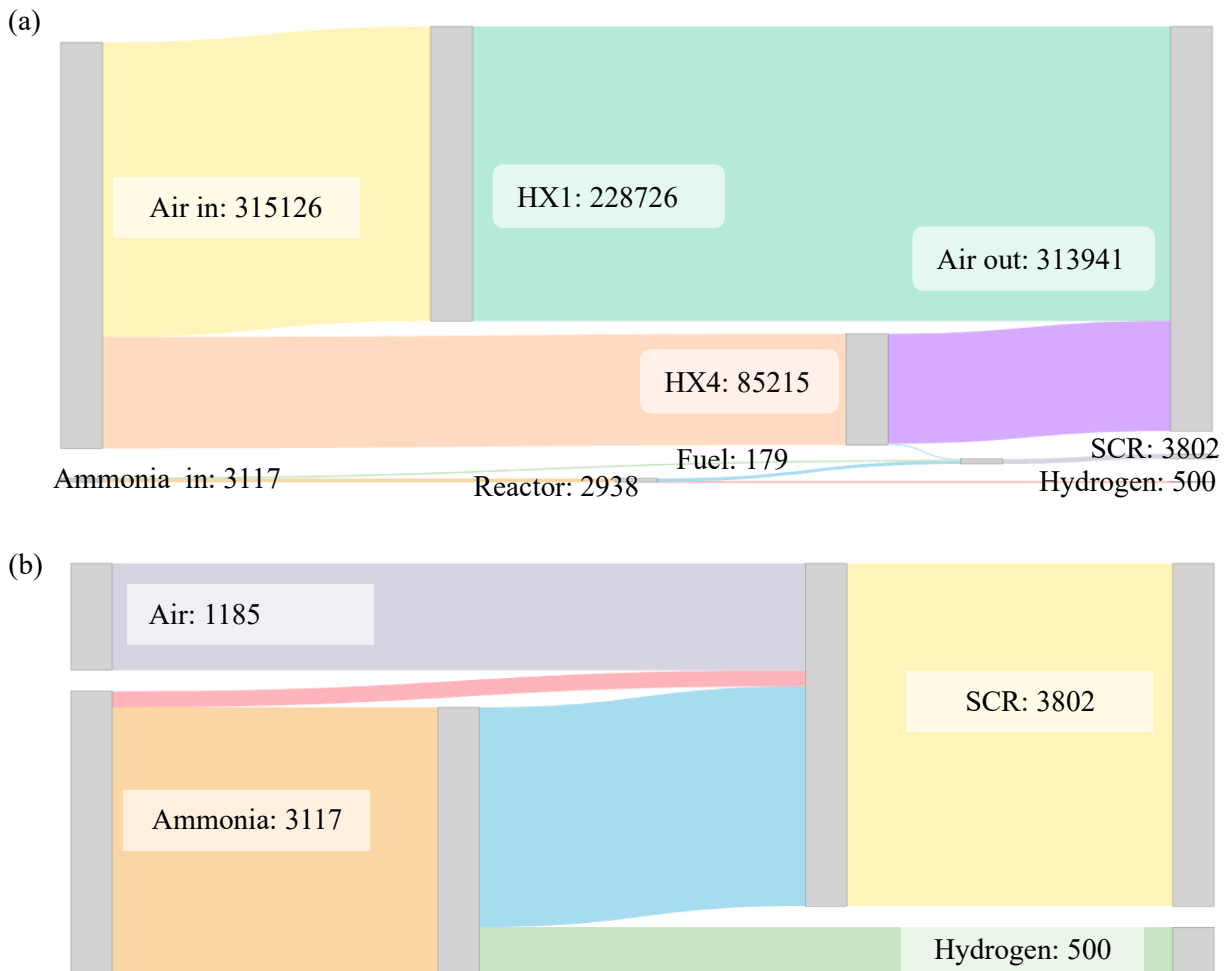


Figure 4.8: Sankey diagram of mass flow through the ammonia decomposition process, (a) entire process and (b) excluding air used in heat exchangers.

Next, an energy Sankey diagram was developed to verify that, in addition to mass conservation, energy is also conserved throughout the process. An energy Sankey diagram is important because it provides a clear visualization of how energy is distributed, transferred, and lost throughout a process.

This insight is crucial for optimizing energy efficiency, improving system design, and reducing operating costs and environmental impact. Figure 4.9 illustrates the energy flow through the ammonia decomposition process using a Sankey diagram. This diagram highlights the distribution of energy across major process units, including compressors, heat exchangers (HX1–HX4), the reactor, combustion chamber, and auxiliary systems such as the selective catalytic reduction (SCR) and cooling stages.

The energy flows are represented as enthalpy changes (in W), calculated using Cantera, which computes species enthalpies relative to a predefined reference state, typically the elemental enthalpies of formation at 298.15 K and 1 atm. As such, negative enthalpy values indicate streams or processes where the enthalpy of the stream is lower than the reference state, typically due to cooling, expansion, or chemical reactions absorbing less energy than the reactants initially contained. Conversely, positive values represent energy inputs or high-enthalpy streams such as combustion or heated products. For instance, the reactor is shown to receive substantial energy input from both HX2 and an external heat source (105,011 W), which is necessary to sustain the endothermic ammonia decomposition reaction. The compressor and cooling systems consume power supplied from the utility stream (shown as 98,467.32 W). The energy Sankey diagram is critical in this context because it provides a transparent and intuitive visualization of where energy is being consumed, recovered, or lost throughout the system. It allows for efficient diagnosis of energy bottlenecks and supports the development of strategies for heat integration, energy recovery, or improved process efficiency.

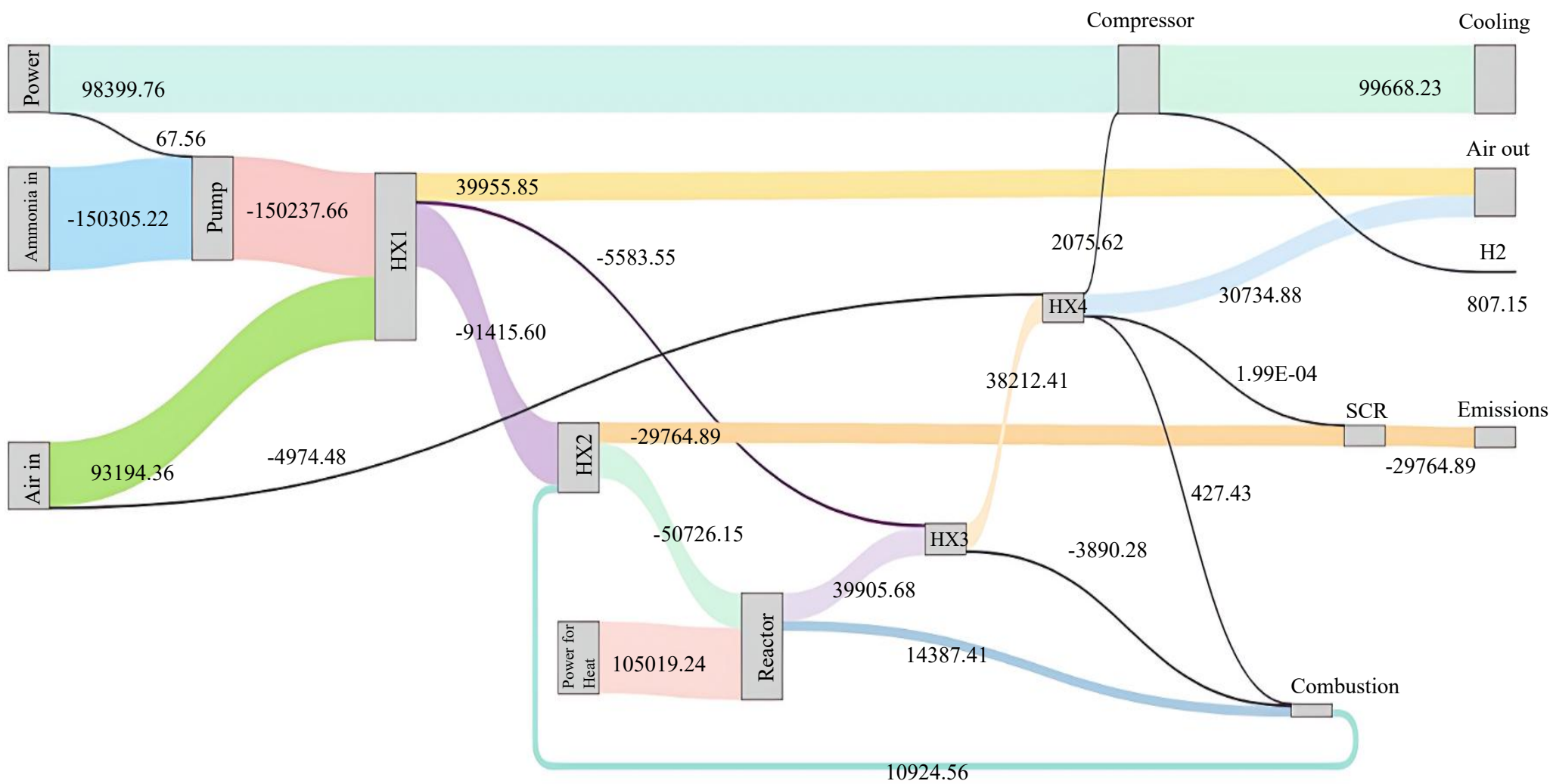


Figure 4.9: Energy flow through ammonia decomposition process.

### 4.3 Economic Analysis

Using capital expenditures (CAPEX), operating expenditures (OPEX) and total revenue generated over the lifespan of the hydrogen refuelling station, an economic analysis was done for the overall process. The purchase cost of all major equipment was found using cost charts from Ulrich and Vasudevan [61]. Since these purchase costs were for 2004, equation 38 and the chemical engineering plant cost index for 2024 (CEPCI, 798.8) were used to get the current purchase cost [62].

$$C_2 = C_1 \left( \frac{I_2}{I_1} \right) \quad (38)$$

The equipment and its cost can be found in Appendix A Table A.9. Figure 4.10 shows the equipment cost breakdown percentage, where approximately 78% of the cost is for buying and installing the compressor at 350 bar.

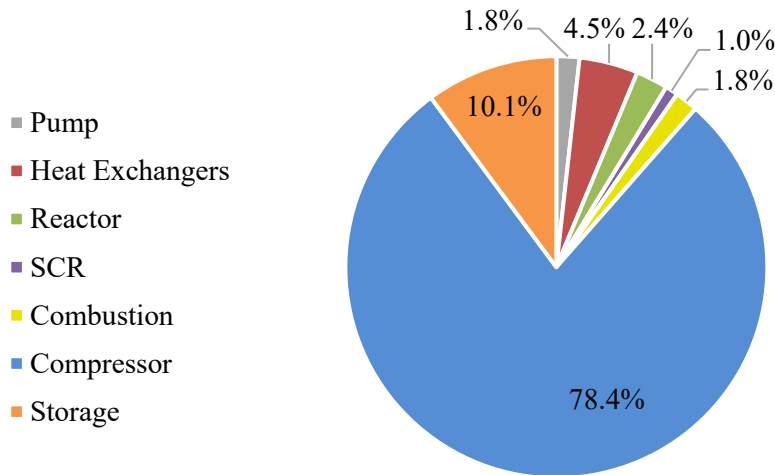


Figure 4.10: Equipment Cost Breakdown.

To estimate the LCOH, the CAPEX, OPEX, and TCI need to be calculated. The following equations (39-42) were used to calculate CRF, CAPEX, LCOH and ROI. The OPEX was calculated by including the cost of consumable materials (catalyst and membrane), utilities, operating labour and supervisor costs, maintenance, local taxes, insurances, and other general expenses.

$$CRF = \frac{i(1+i)^{n_{pl}}}{(1+i)^{n_{pl}} - 1} \quad (39)$$

$$CAPEX = CRF \times TCI \quad (40)$$

$$LCOH = \frac{(CRF \times TCI) + OPEX}{Annual\ Production\ Capacity} \quad (41)$$

$$ROI = \frac{Annual\ profit}{TCI} * 100 \quad (42)$$

A summary of the CAPEX and OPEX is given in Tables 4.5 and 4.6. In addition, any assumptions and additional costs, such as consumables, are listed in Table 4.4.

Table 4.4: Assumptions applied for LCOH estimation in the base case.

Parameters	Value	Reference
Ammonia cost, CAD/kg	0.60	[63]
Cooling water, CAD/m <sup>3</sup>	3.14	[64],[65],[66]
Electricity cost, CAD/kWh	0.11	[67]
Discount rate, %	10.0	[50]
Plant working days, days/year	350	-
Plant life, years	20	-
Catalysts (ammonia cracker), CAD/kg	35.0	[68]
Catalyst (SCR), CAD/ m <sup>3</sup>	8203.5	[69]
Lifetime ammonia cracker catalyst	5	[32]
Lifetime SCR catalyst	5	[32]
Membrane (Pd-based), CAD/ m <sup>2</sup>	3126.8	[68]
Number of Labour	5.00	-
Labour cost, \$/hour	21.0	[70]

The fixed capital investment, working capital investment, and total capital investment for this process were estimated using established economic factors for chemical process plants, which can be found in Table 4.5. When calculating the capital expenditure, the CRF was calculated to be around 0.12.

Table 4.5: Estimation of total capital investment cost [50].

<b>Parameters</b>	<b>Factor, %</b>	<b>Cost, CAD</b>
Fixed Capital investment	504	1.41e6
<u>Direct Costs</u>		
Purchased equipment cost	100	2.79e5
Installation cost, including insulation and painting	47.0	1.31e5
Instrumentation and controls (installed)	36.0	1.01e5
Piping cost (installed)	68.0	1.90e5
Electrical system (installed)	11.0	3.07e4
Buildings, including all facilities	18.0	5.03e4
Yard improvements	10.0	2.79e4
Service facilities (installed)	60.0	1.68e5
Total direct plant cost	350	9.77e5
<u>Indirect Costs</u>		
Engineering and supervision	33.0	9.21e4
Construction expenses	41.0	1.14e5
Legal expenses	4.00	1.12e4
Contractor's fee	22.0	6.14e4
Contingency	44.0	1.23e5
Total indirect plant cost	144.0	4.02e5
Working capital investment (WCI)	89.0	2.48e5
Total capital investment	593	1.63e6
<u>Capital expenditure</u>	-	1.91e5

After calculating the capital investment of the plant, further calculations for operating cost were performed using the cost of consumable material, operating labour cost, and utilities. All these costs are summarized in Table 4.6. The cost of consumables includes the cost of replacing the membrane, the catalyst and the ammonia feedstock for the year. The utilities include the cost of electricity and water supply for the year to cool down between stages in the multi-stage compressor.

Table 4.6: Estimation of total production cost.

<b>Parameters</b>	<b>Factor</b>	<b>Cost (CAD/year)</b>
<u>Direct production costs</u>		
Consumable material costs ( $C_{RM}$ )	$1.00 \times C_{RM}$	8.40e5
Operating labour cost ( $C_L$ )	$1.00 \times C_L$	1.76e5
Direct supervision cost ( $C_S$ )	$0.15 \times C_L$	2.65e4
Utilities ( $C_U$ )	$1.00 \times C_U$	4.95e4
Maintenance ( $C_M$ )	$0.06 \times FCI$	8.44e4
Operating supplies ( $C_{OS}$ )	$0.15 \times C_L$	2.65e4
Total direct production costs	$C_{RM} + 1.30 C_L + C_U + 0.06 FCI$	1.20e6
<u>Fixed charges</u>		
Local taxes ( $C_{LT}$ )	$0.025 \times FCI$	3.52e4
Insurance ( $C_I$ )	$0.007 \times FCI$	9.85e3
Financing ( $C_F$ )	$0.1 \times TCI$	1.63e5
Total fixed charges	$0.032 FCI + 0.1 TCI$	2.08e5
Plant overhead costs	$0.6325 C_L + 0.033 FCI$	1.58e5
Total manufacturing costs	$C_{RM} + 1.9325 C_L + C_U + 0.125 FCI + 0.1 TCI$	1.57e6
<u>General expenses</u>		
Administrative costs ( $C_A$ )	$0.23 C_L + 0.012 FCI$	5.75e4
<u>OPEX</u>	$C_{RM} + 2.1625 C_L + C_U + 0.137 FCI + 0.1 TCI$	1.63e6

The levelized cost of hydrogen for this refuelling station was calculated to be \$10.38/kg H<sub>2</sub>, which can vary depending on variable costs such as the price of ammonia, energy consumption, labour, and utilities. The LCOH can be broken down into CAPEX and OPEX, where the operating costs can be split into direct production costs and fixed costs. This is represented in Figure 4.11.

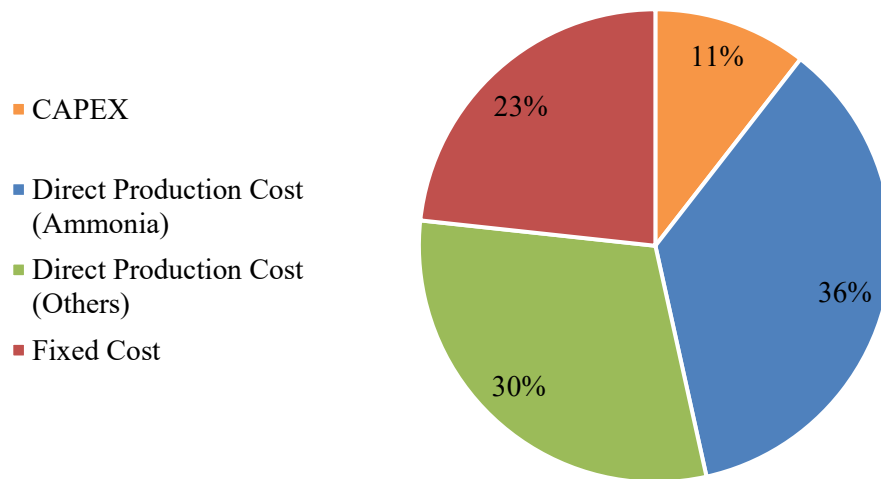


Figure 4.11: LCOH breakdown.

Currently, in Canada, the only publicly available price of hydrogen for refuelling stations is from HTEC in British Columbia, which prices its hydrogen from \$14.75 to \$16.50 per kg [71]. In the US last year, the average price per kg in USD was between \$13 and \$22 (CAD \$19.03-29.93) depending on the state. However, as of this year in March 2025, the average price rose to USD \$34/kg (CAD \$46.24/kg) [72]. The reason for this large range in price is due to higher retail markups, distribution costs, and profit margins.

When comparing the LCOH for different hydrogen production methods, it is important to consider how each system boundary is defined and the output condition, such as the final hydrogen pressure. Most LCOH estimates do not include the additional cost of compressing hydrogen to the pressures required for various end-use applications. For example, in this thesis, the end-use application was for heavy-duty vehicles at refuelling stations, which require 350 bar. In literature for ammonia cracking processes using PSA, the LCOH ranges from \$7.54-8.57/kg [33] [50] [19] with a hydrogen output pressure of 1 atm. Another study from Makloufi et al. [49] calculated the LCOH to be \$9.03/kg with an output of 250bar for hydrogen. Even with the LCOH in this thesis being higher when compared to those in literature, it is due to the fact that the final pressure of hydrogen as the compressor adds a considerable amount of cost to capital and production cost. When comparing the LCOH to current market prices, it is feasible if the price of hydrogen in the refuelling station in Ontario is set to \$16.50/kg. The ROI was calculated to be 27.05%. Since it is higher than the finance interest rate of 10% and the minimum acceptable ROI, as described in general practice.

When comparing to the traditional methods of producing steam methane reforming (SMR), the LCOH for steam methane reforming ranges from \$2.06-3.43/kg [51] and with carbon capture \$2.75-4.80/kg [51] if the hydrogen output was at 1 atm. When comparing LCOH of ammonia cracking to SMR with and without a carbon capture system, it is usually cheaper to use SMR as it leverages an already mature, efficient and fossil-fuel-based industrial process. In addition, the feedstock, which is natural gas, is a lot cheaper than using ammonia as the feedstock. However, if we want to use a cleaner production method, other methods should be used.

## 4.4 Environmental analysis

In literature, Cho et al [38] mentioned that there have been disagreements among the reviewed studies for ammonia decomposition process data and system boundaries. For example, a study by Dickson et al. [73] performed ammonia decomposition at 450 °C and 1 atm, which required 14.3 kWh/kg H<sub>2</sub> of energy, whereas Noh et al. [74] mentioned they needed 9.4 kWh/kg H<sub>2</sub> for the decomposition in spite of much higher energy-intensive reaction conditions of 900 °C and 40 bar. The energy required for decomposition is significantly influenced by the type of catalyst, particularly its activity and optimal reaction temperature, which directly impact the ammonia conversion rate and hydrogen recovery [82]. Figure 4.12 compares ammonia decomposition in this thesis and the electricity consumption of other hydrogen production processes, such as steam methane reforming and electrolysis. As seen in Figure 4.12, electrolysis requires a massive amount of energy (electricity) to produce 1 kg of hydrogen, while the other hydrogen production methods have very similar electricity consumption. The exact values and references for this can be found in Appendix A, Table A.7. Currently, for the base case, 9.77 kWh/kg H<sub>2</sub> is required. In this amount, currently 5.04 kWh/kg H<sub>2</sub> in electricity is needed to maintain isothermal conditions in the reactor. However, if heat from the ammonia combustion unit is used instead of electricity, then the electricity consumption lowers to 4.73 kWh/ kg H<sub>2</sub>. The majority of the electricity consumption comes from maintaining a high temperature for the ammonia cracker and for hydrogen compression. Typically, producing compressed hydrogen requires 1 kWh/kg H<sub>2</sub> to 7 kWh/kg H<sub>2</sub> of compressed hydrogen [75]. In this process, approximately 4.72 kWh/kg is needed to reach 350 bars.

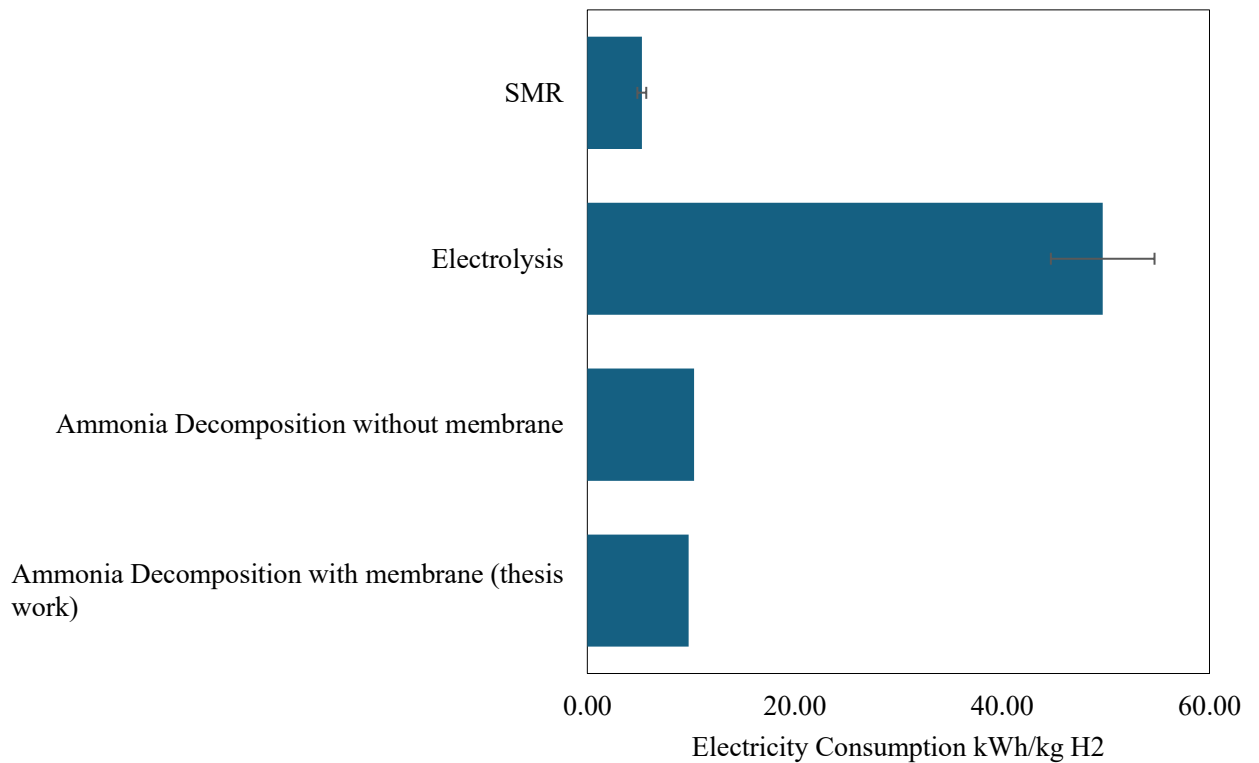


Figure 4.12: Electricity consumption of hydrogen production paths.

The carbon footprint of a process is determined by factors such as electricity consumption, the energy source (e.g., fossil fuels vs. renewables), direct CO<sub>2</sub> emissions, and the supply chain and transportation of raw materials. In this thesis, the CO<sub>2</sub> emissions considered are from the electricity grid, transporting ammonia and the associated emissions related to the feed source (ammonia). While ammonia decomposition does not produce any direct CO<sub>2</sub>, it requires electricity, making the emissions associated with the process dependent on the electricity source. This model assumes that electricity is sourced from the Ontario electricity grid, which has an emission intensity of 29 g CO<sub>2</sub>e/kWh [55]. The carbon emission from using electricity in this process is 0.28 kg CO<sub>2</sub>e/kg H<sub>2</sub>. However, this depends on where the process is placed and the electricity grid. If the electricity comes from burning natural gas, then the emissions would be a lot higher than when compared to using renewable energy. In this process, there are also carbon emissions from transporting the ammonia to the refuelling station. The carbon dioxide emissions per tonne of km transported are 11.94 and 73.92 g CO<sub>2</sub>e / tonne-km for rail and truck, respectively. Assuming ammonia is being transported from a green ammonia production plant in Point Tupper, Nova Scotia, to Kitchener, Ontario (1968km) by rail and truck, the final total carbon emissions are 0.15kg CO<sub>2</sub>e/ kg H<sub>2</sub>. Finally, the emissions associated with the feed were also included. Currently, the carbon emissions associated with green ammonia is

0.71 kg CO<sub>2e</sub>/ kg NH<sub>3</sub> [76], making the emissions related to ammonia for this process 4.43 kg CO<sub>2e</sub>/ kg H<sub>2</sub>. From all this, the total carbon emission associated with this process in this thesis is 4.86 kg CO<sub>2e</sub>/ kg H<sub>2</sub>. When comparing the carbon emissions from other hydrogen production methods, it is still lower than using steam methane reforming, coal gasification and electrolysis from the global grid. However, with carbon capture methods or renewable electricity sources being used, the carbon emissions become very similar to the ammonia decomposition process. The majority of the carbon emissions come from the emissions associated with the feed. Therefore, to further reduce this value, upstream methods need to be improved for emission reduction. The exact values for each type of hydrogen production method and CO<sub>2</sub> emissions can be found in Appendix A, Table A.8.

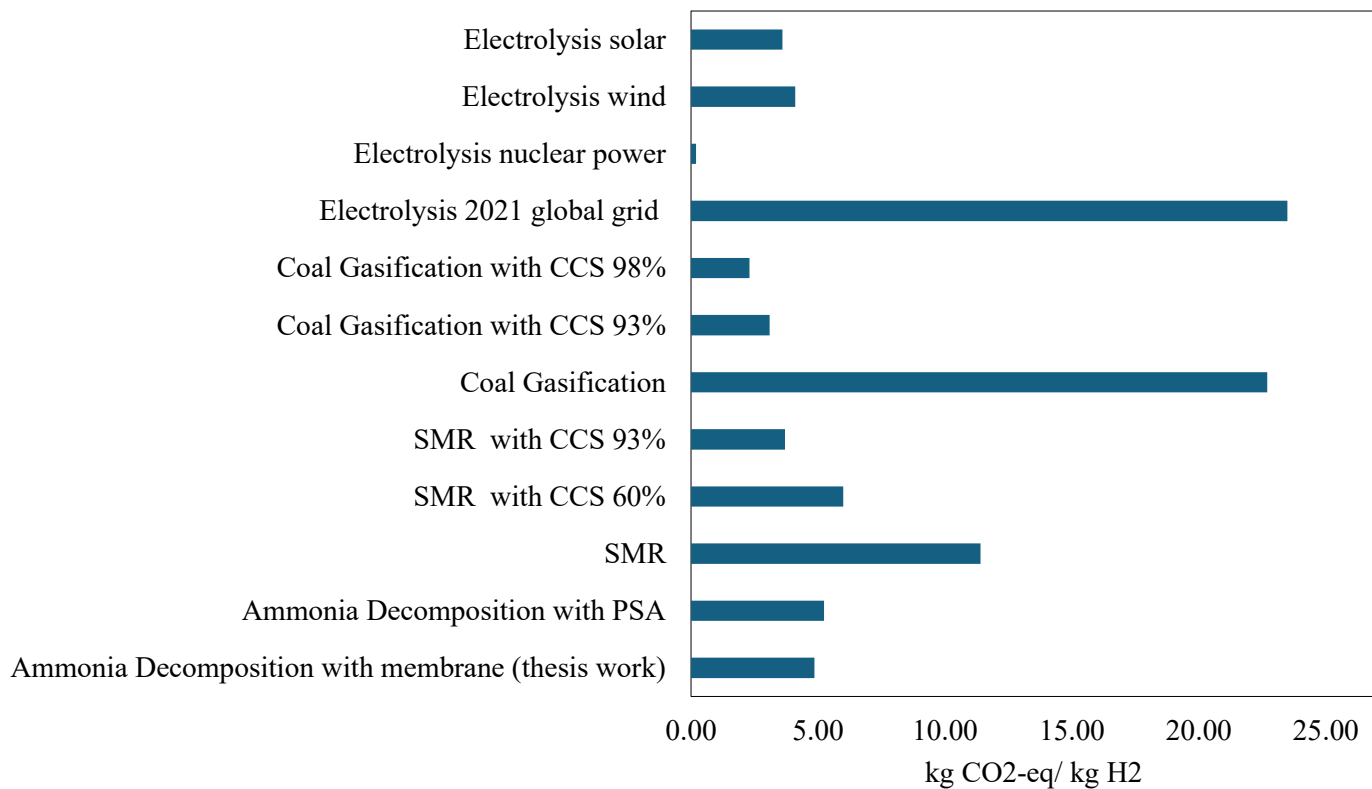


Figure 4.13: CO<sub>2</sub>-equivalent emissions per kilogram of hydrogen for various production methods (Appendix A Table A.8).

The NO<sub>x</sub> emissions come from the furnace when ammonia is combusted, which includes NO, NO<sub>2</sub> and N<sub>2</sub>O. In Ontario, the regulation of nitrogen oxides (NO<sub>x</sub>) emissions from combustion sources, such as ammonia-fired furnaces, is governed by the Ministry of the Environment, Conservation and Parks (MECP). While specific NO<sub>x</sub> emission limits for ammonia combustion furnaces are not explicitly detailed in publicly available guidelines, general standards and criteria apply. Guide A-9:

NO<sub>x</sub> Emissions from Boilers and heaters provides recommended NO<sub>x</sub> emission limits for various combustion devices. Although it primarily addresses boilers and heaters using conventional fuels, the principles may apply to ammonia combustion processes. The guideline emphasizes the implementation of Best Available Control Technology (BACT) to minimize emissions [40]. In Ontario, they outline limits for NO<sub>2</sub> and N<sub>2</sub>O in the Ambient Air Quality Criteria report, which was developed by the Ontario Ministry of the Environment (MOE). Table 4.7 shows the limit of how much nitrous oxide and nitrogen dioxide can be emitted into the air. Anything above this limit is unacceptable, and another device is needed to reduce these emissions.

Table 4.7: Ambient Air Quality Criteria NO<sub>2</sub> and N<sub>2</sub>O [41].

Contaminant	AAQC (µg/m <sup>3</sup> )	Averaging Time
NO <sub>2</sub>	200 (0.1ppm)	24 hours
	400 (0.2 ppm)	1 hour
N <sub>2</sub> O	9000	24 hours

In addition, the Ontario Regulation 419/05 (Air Pollution – Local Air Quality), which is under the Environmental Protection Act of Ontario, sets limits on air pollutant concentrations at the point where emissions from a facility reach human receptors or the environment. This is done to protect local air quality and human health. Although the emissions from this process were well below regulatory limits, a selective catalytic reduction (SCR) system was implemented as a best practice to minimize nitrogen oxide emissions. This aligns with the long-term goal of deploying multiple hydrogen refuelling stations across Ontario and Canada to support the growing demand for fuel cell electric vehicles (FCEVs). Figure 4.8 shows the results for the base case for NO<sub>x</sub> emissions.

Table 4.8: Base case results for NO<sub>x</sub> emissions.

Parameters	Inlet SCR (µg/m <sup>3</sup> )	Outlet SCR (µg/m <sup>3</sup> )
Amount of Nitric Oxide	0.09	0.03
Amount of Nitrogen Dioxide	5.37e-5	5.37e-5
Amount of NO <sub>x</sub>	0.09	0.03
Temperature (K)	376.9	

# Chapter 5 Sensitivity Analysis

To better understand the ammonia cracking system and its behaviour under different operating conditions, a sensitivity analysis was conducted. This analysis aimed to evaluate how changes in key parameters, such as temperature, pressure, and membrane permeance, can influence the system's outcomes. This includes hydrogen yield, ammonia conversion efficiency, overall electricity consumption, and LCOH. By identifying which parameters have a significant impact on the system, it can provide valuable insights for optimizing the process and driving future design and operational decisions.

## 5.1 Impact of process variables on system outputs

The first part of this sensitivity analysis focuses on varying three key parameters, which are pressure, temperature and membrane permeance. These parameters were chosen as they have a direct significant impact on the reactor performance. Pressure was examined as it influences the equilibrium conversion and membrane driving force. Temperature is also critical as the ammonia decomposition reaction is highly endothermic and strongly temperature-dependent. Lastly, membrane permeance was chosen because it directly affects the rate at which hydrogen can be selectively removed from the reaction zone. The reactor dimensions were kept the same as the base case scenario. In Table 5.1 are the parameters and the range in which the variables were tested.

Table 5.1: Parameters and values used in the sensitivity analysis.

Parameters	Range
Pressure	4.00-16.0 bar
Temperature	400-600 K
Membrane Permeance	4.00e-10 – 9.00e-9 kmol/m <sup>2</sup> s Pa

### 5.2.1 Pressure

Sufficient pressure is very important to maintain hydrogen permeation across the membrane. As mentioned before, hydrogen is selectively removed from the reaction mixture through the membrane. Sievert's law can describe the hydrogen flux through the membrane. In this case, Sievert's law is applied with an exponent  $n=1$ , meaning the hydrogen flux across the membrane is directly proportional to the difference in partial pressures of hydrogen between the retentate and permeate sides. Therefore, increasing the pressure difference between the two sides of the membrane directly

enhances the driving force. As a result, a higher retentate pressure while keeping the permeate side pressure improves hydrogen recovery. This effect can be clearly observed when the sweep side (permeate) pressure is maintained around 1 atm. At low retentate pressures, the pressure differential is small, and the hydrogen recovery is limited. For example, at a retentate pressure of approximately 4 bar, the hydrogen recovery is around 50%. However, when the retentate pressure is increased to 16 bar, the hydrogen recovery approaches 98%. From these results, it can be seen how important it is to have a bit higher pressure on the retentate side in membrane reactors. While operating at higher retentate pressures improves hydrogen recovery, it also increases the overall system pressure, which can lead to higher energy consumption and may require additional safety measures and more robust equipment to handle higher operating conditions.

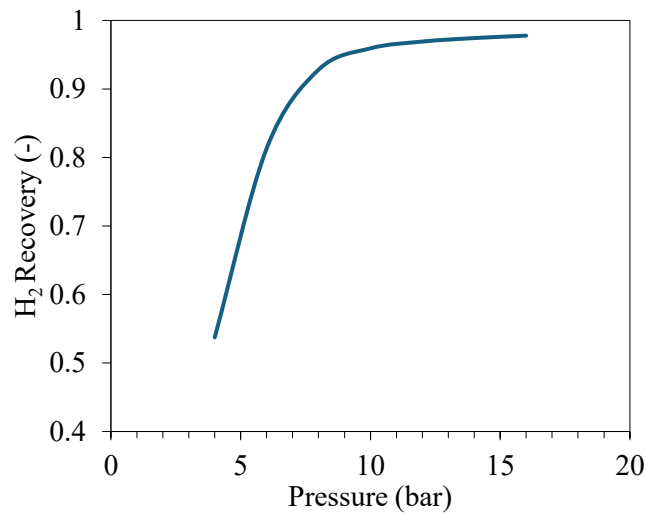


Figure 5.1: Influence of retentate pressure on hydrogen recovery (permeate side pressure is kept at 1 bar).

In typical packed bed reactors, ammonia decomposition is favoured at lower pressures, as during the reaction, the number of moles increases. However, in a membrane reactor, hydrogen is continuously removed from the reaction zone to the permeate side. This removal shifts the reaction equilibrium forward, which explains the slight increase in ammonia conversion seen in Figure 5.2. Beyond a certain point (10 bar) the conversion increase becomes marginal, and the curve begins to level off.

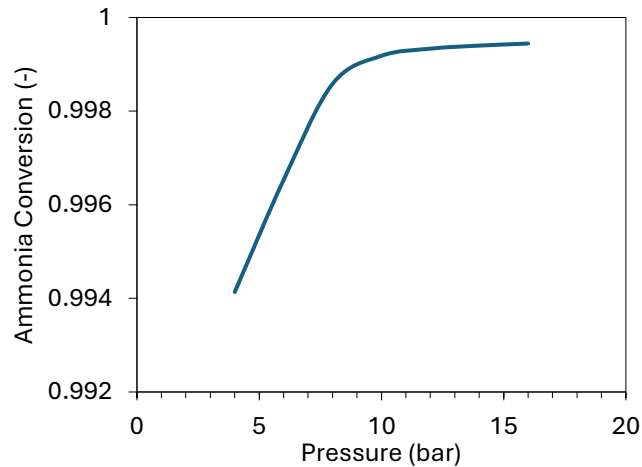


Figure 5.2: Influence of pressure on ammonia conversion.

Although operating at higher retentate pressures enhances hydrogen recovery, this benefit must be balanced against associated drawbacks such as increased electricity demand. In evaluating the overall impact of the operating pressure on the reactor, it is important to consider the electricity demand per kilogram of hydrogen produced. The added electricity by increasing the pressure is relatively minor when compared to the significant improvement in hydrogen recovery achieved at higher pressures. Therefore, with an increase in hydrogen permeation efficiency, the extra compression energy is offset, resulting in a decrease in energy consumption per kg H<sub>2</sub> produced as the pressure increases. Therefore, from a process optimization perspective, increasing the retentate pressure not only improves hydrogen separation and supports high ammonia conversion but also contributes to a more energy-efficient system.

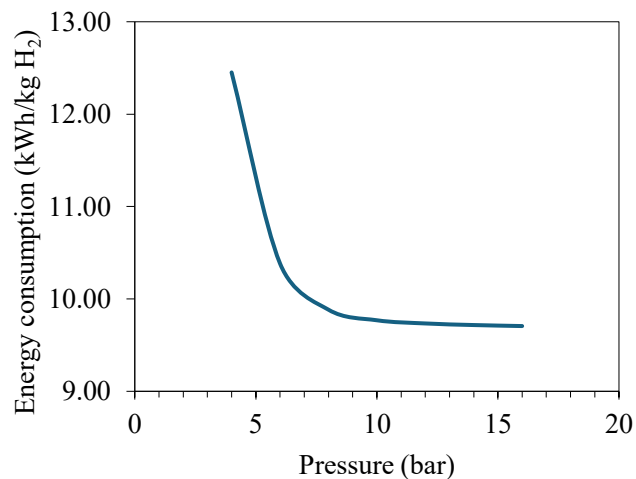


Figure 5.3: Influence of pressure on electricity consumption.

## 5.2.2 Temperature

Temperature plays a critical role in the performance of the ammonia cracker, mainly due to the thermodynamic nature of the reaction. As mentioned previously, this reaction is endothermic, meaning it requires heat input to proceed. When looking into Le Chatelier's principles, increasing the temperature shifts the reaction equilibrium toward the products, which in this case are nitrogen and hydrogen. Therefore, higher operating temperature promotes excellent ammonia conversion, which in turn increases the amount of ammonia and the amount of hydrogen available for separation. This can be seen in Figure 5.4, where with an increase in temperature, the hydrogen recovery also increases. The same trend can be seen in Figure 5.5, where with an increase in temperature, the ammonia conversion increases. It is also important to note that temperature has a greater effect on the ammonia conversion than pressure. At lower temperatures (below 450°C), the ammonia conversion and hydrogen recovery remain relatively low due to limited reaction kinetics. Once the temperature exceeds approximately 450°C, both conversion and recovery begin to improve rapidly. Beyond this point, however, the rate of improvement starts to level off as it reaches close to 100%. This suggests that after a certain temperature threshold, the system approaches thermodynamic equilibrium and mass transfer limits.

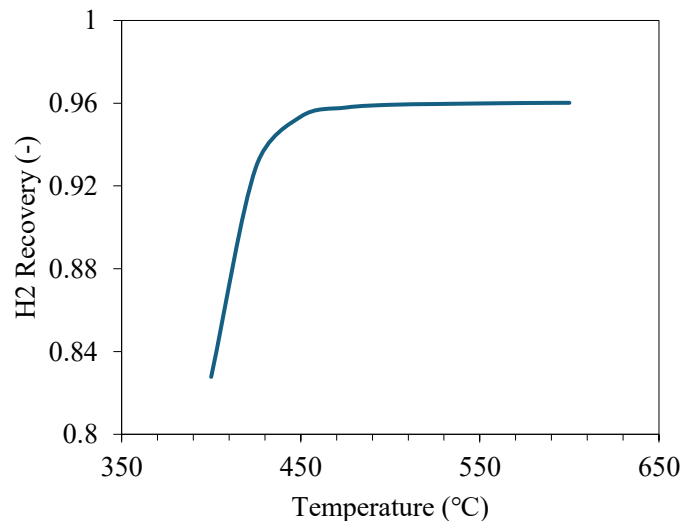


Figure 5.4: Influence of temperature on hydrogen recovery.

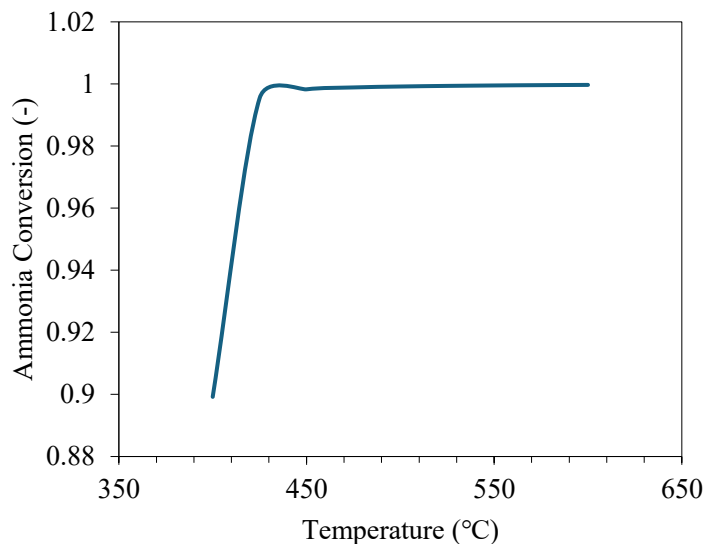


Figure 5.5: Influence of temperature on ammonia conversion.

While higher temperatures improve both ammonia conversion and hydrogen recovery, they also come with trade-offs such as more energy demand. Since ammonia decomposition is endothermic, operating at higher temperatures requires a larger pre-heat requirement and a greater heat input to maintain the temperature in the reactor at isothermal conditions. In addition to the increase in energy needed to heat up the reactor, there is also a higher demand on the compressor since more hydrogen is being recovered. Therefore, there will also be an increase in electricity demand. However, as highlighted earlier, higher temperatures lead to more complete ammonia conversion and improved hydrogen yield, which means that although more electricity is being used, a greater quantity of usable hydrogen is obtained. The key, therefore, lies in finding an optimal temperature range where the gains in conversion and recovery outweigh the additional electricity costs. This balance point typically occurs beyond 450°C, where system performance improves significantly, but the benefits begin to level off, suggesting diminishing returns on energy input at excessively high temperatures.

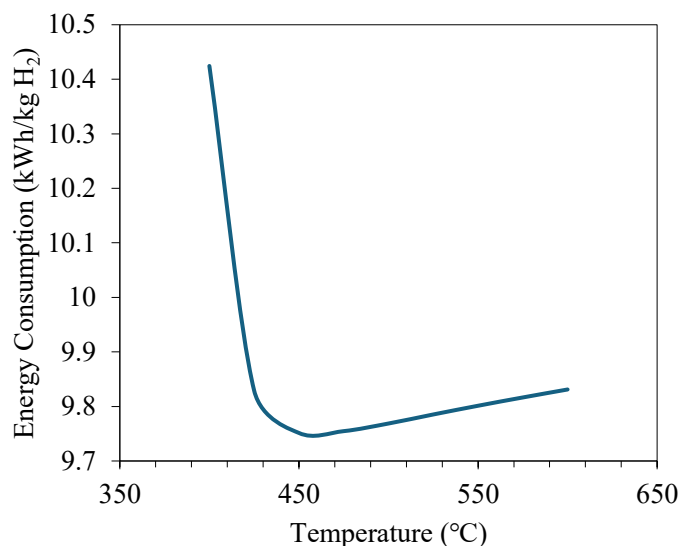


Figure 5.6: Influence of temperature on electricity consumption.

### 5.2.3 Membrane Permeance

Having explored the influence of pressure and temperature on the ammonia decomposition membrane reactor, another important parameter to consider is the membrane permeance, which directly affects hydrogen recovery. Membrane permeance is a measure of how easily a gas can pass through the membrane material, and it is typically calculated using the membrane's permeability and thickness. As seen in Figure 5.7, increasing membrane permeance significantly improves the system performance, particularly in terms of hydrogen yield. While high permeance is clearly advantageous from a process standpoint, it is not always practically achievable. The permeance depends on the material properties and fabrication quality of the membrane. For example, dense palladium-based membranes exhibit high hydrogen selectivity and permeability but can be expensive, fragile, and sensitive to contaminants. Composite membranes or ceramic-supported palladium membranes can offer improved mechanical stability, but often at the cost of reduced permeance. Furthermore, membrane thickness cannot be decreased randomly to improve permeance, as thinner membranes may suffer from mechanical failure, reduced durability, or pinhole formation. Therefore, a trade-off exists between achieving high permeance and maintaining membrane integrity and longevity. Additionally, different materials may exhibit different temperature-dependent permeability behaviours, meaning that the effectiveness of the membrane may vary with operating conditions.

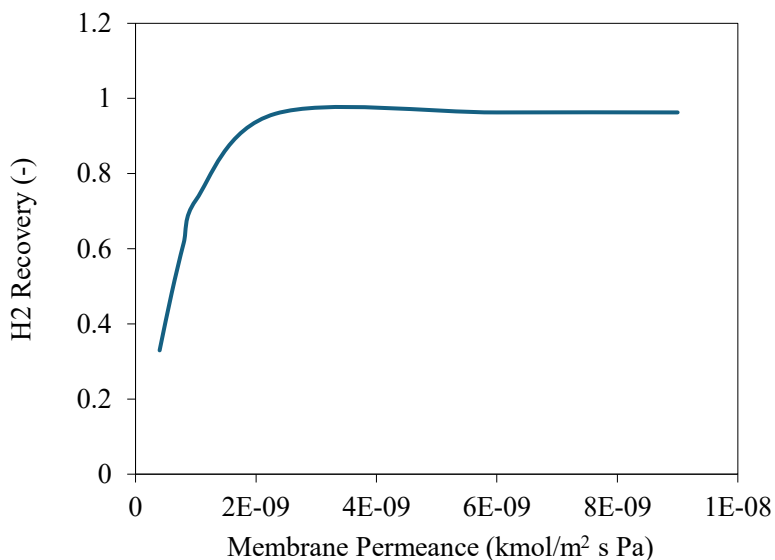


Figure 5.7: Influence of membrane permeance on hydrogen recovery.

A higher membrane permeance enables more efficient removal of hydrogen from the reaction zone, which thermodynamically drives the equilibrium forward and promotes greater ammonia decomposition. In this specific case, the reactor was designed with sufficient length to allow the system to already achieve near-complete ammonia conversion, even under baseline conditions. Because the hydrogen was being effectively removed over the course of the reactor length, the system was already operating close to its thermodynamic and kinetic limits. As a result, increasing the membrane permeance beyond a certain point provided only marginal gains in ammonia conversion, since most of the ammonia had already decomposed. While higher permeance generally enhances conversion by improving hydrogen removal and equilibrium shifting, its impact becomes less pronounced when the reactor is long enough (in this case 1.6m) to allow the reaction to proceed nearly to completion. This highlights an important design consideration: the benefits of increasing membrane permeance must be evaluated in the context of reactor dimensions and operating conditions. Beyond a certain threshold, further improvements in permeance may yield diminishing returns in terms of conversion, and optimization efforts might be better focused on other aspects of the system.

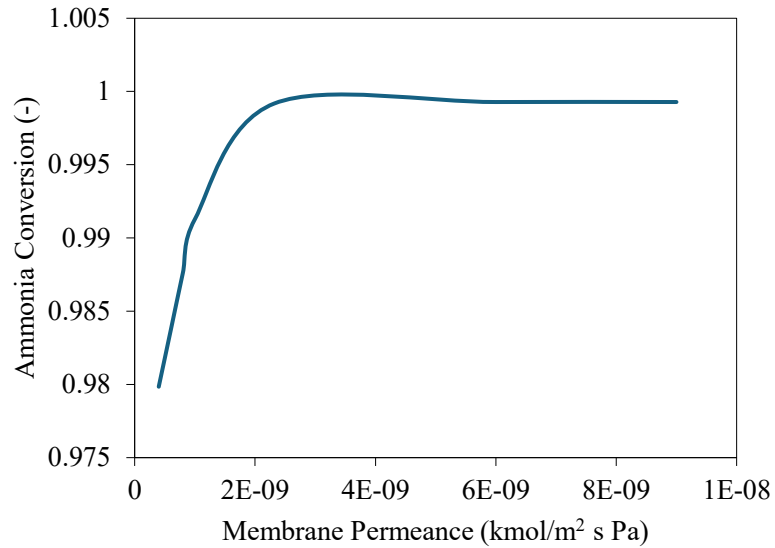


Figure 5.8: Influence of membrane permeance on ammonia conversion.

The primary factor influencing electricity demand is the amount of hydrogen that permeates through the membrane, as it directly affects the load on the downstream compressor. Since the reactor operates at a fixed temperature (under isothermal conditions), changes in membrane properties do not alter the energy needed to maintain reactor temperature. However, as the membrane permeance increases, more hydrogen is removed from the retentate side and transferred to the permeate side. This means a greater volume of hydrogen must be compressed to reach the desired utilization pressure, which increases the energy demand of the compressor. Despite this increase in compression work, the system becomes more energy-efficient overall. With more hydrogen being recovered, the specific energy consumption tends to decrease. This is because the increase in hydrogen output outweighs the additional compression energy required. Therefore, even though compressor energy rises with higher permeance, the system delivers more usable hydrogen, improving the net energy performance.

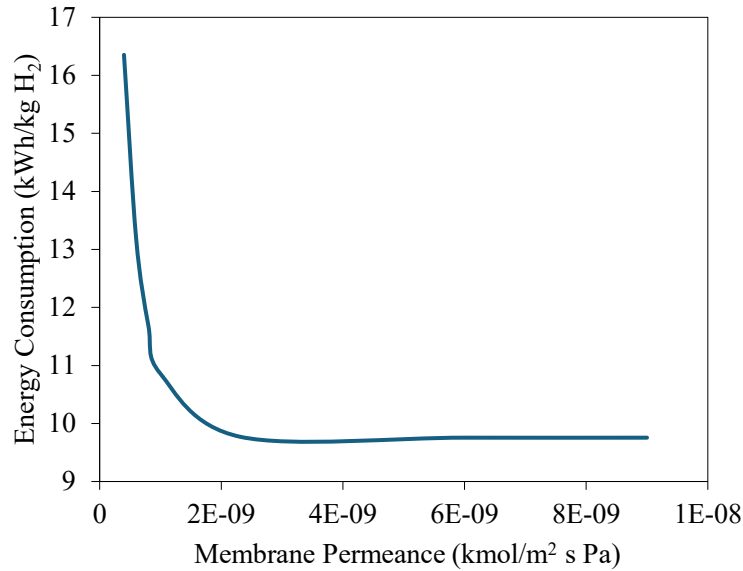


Figure 5.9: Influence of membrane permeance on energy consumption.

## 5.2 Sensitivity analysis on NO<sub>x</sub> emissions

The equivalence ratio is a key parameter in combustion processes and represents the ratio of actual fuel-to-air mixture to the stoichiometric ratio. An equivalence ratio less than one indicates a lean mixture (excess air) while a value greater than one signifies a rich mixture (excess fuel). This balance of fuel and air significantly impacts the formation of nitrogen oxides and nitrogen dioxide during ammonia combustion. Under lean conditions, especially at equivalence ratios around 0.8, the concentration of both NO<sub>x</sub> and NO<sub>2</sub> emissions is observed to be at its highest. This is because the combustion environment has excess oxygen, creating a strong oxidizing atmosphere. Such conditions favour the formation of NO<sub>x</sub> and N<sub>2</sub>O as more oxygen is available to react with nitrogen, and intermediate reaction pathways occur. As the equivalence ratio increases beyond one and the combustion becomes fuel-rich, the availability of free oxygen decreases. It is important to note that these emission results reflect the exhaust gas composition immediately after combustion. However, in practical application, a post-combustion treatment system, such as a selective catalytic reduction unit, is installed downstream of the combustion zone. In this system, an SCR was used to remove up to 85% of NO and N<sub>2</sub>O when operated under optimal conditions. This significantly lowers the final NO<sub>x</sub> emissions released to the atmosphere, helping the system meet environmental regulations. Their results highlight the critical influence of the equivalence ratio on pollutant formation during ammonia combustion and the importance of integrated emissions control strategies such as operating under fuel-rich conditions and using SCR to minimize environmental impact. In the base case scenario, 0.94

was used; however, for future designs, a higher equivalence value should be used to minimize  $\text{NO}_x$  emissions. Figure 5.10 shows how increasing the equivalence value minimizes these emissions.

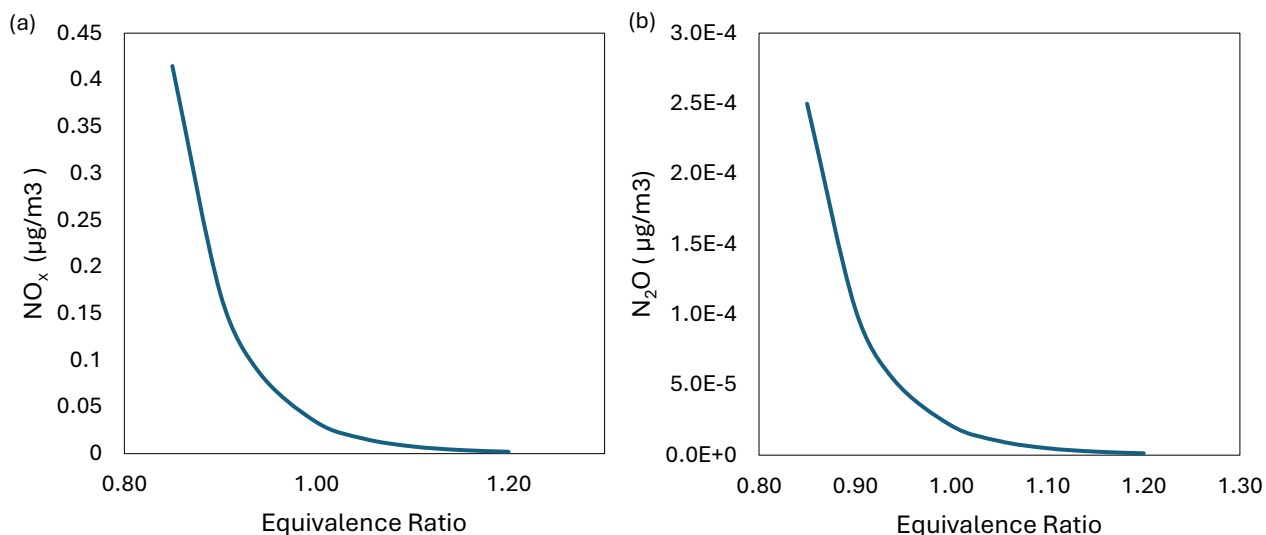


Figure 5.10: Influence of equivalence ratio on  $\text{NO}_x$  and  $\text{N}_2\text{O}$  concentration.

### 5.3 Sensitivity analysis of the levelized cost of hydrogen

In addition to doing a sensitivity analysis on key reactor parameters and equivalence ratio, a sensitivity analysis was performed on the LCOH. This was done to better understand the economic robustness of the ammonia decomposition system and identify which parts of the process contribute most to the LCOH. The results are illustrated in Figure 5.11, which shows how variations in individual cost parameters influence the final LCOH. Each parameter was varied independently by  $\pm 30\%$  from its baseline value (these values can be found in Table 4.4-4.6), while all other parameters were held constant. Each bar reflects the effect of increasing (in red) and decreasing (in blue) for the corresponding input parameter. From the chart, it is evident that the price of ammonia is the most significant factor affecting the LCOH. A  $\pm 30\%$  change in ammonia price shifts the LCOH over a wide range of approximately \$9.3-11.5/kg  $\text{H}_2$ . Other impactful factors that affect the LCOH are labour costs and the compressor. Parameters such as catalyst cost, membrane price, and maintenance have a moderate impact, while utility cost and reactor cost show only a minor influence on the overall hydrogen cost. This suggests that optimization efforts and cost-reduction strategies should primarily focus on the feedstock procurement, labour efficiency and compressor design.

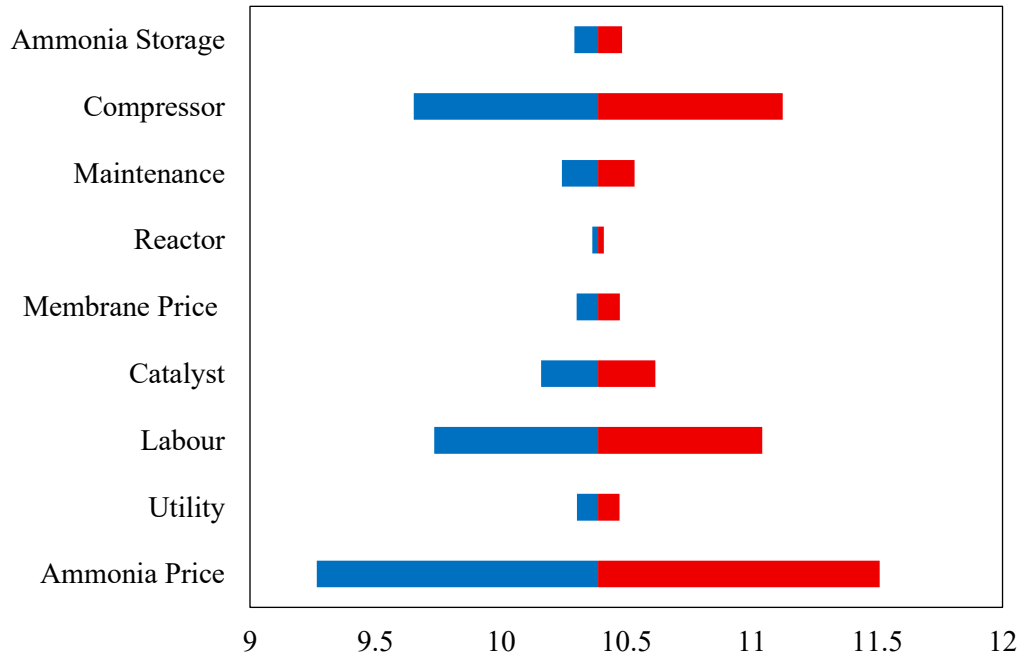


Figure 5.11: Impact of  $\pm 30\%$  variations in capital and operating cost parameters on the Levelized Cost of Hydrogen (LCOH).

Figure 5.12 illustrates how three critical process parameters previously examined (pressure, temperature, and membrane permeance) affect the LCOH in the ammonia decomposition system. These plots provide insight into the system's sensitivity to operating conditions and help identify optimal ranges for minimizing hydrogen production costs. In Figure 5.12(a), the LCOH is shown to decrease significantly with increasing retentate pressure, especially between 4 and 8 bar. This is due to more hydrogen permeating through the membrane, which improves hydrogen recovery. As more hydrogen is recovered without substantially increasing capital or operational costs, the cost per kilogram of hydrogen declines. However, beyond approximately 10 bar, the curve begins to flatten, as the amount of hydrogen produced becomes constant. In Figure 5.12 (b), the LCOH is also shown to decrease with an increase in temperature. As mentioned previously, increasing the temperature increases ammonia conversion and the hydrogen recovery. If the capital and operating costs remain relatively constant, then an increase in hydrogen production will result in a decrease in the LCOH. Beyond 500K, the LCOH flattens as the reaction has already reached near-complete conversion, and additional thermal input provides little change in terms of cost reduction. From this, it is suggested that the optimal temperature range exists typically between 450-500K, where the performance is maximized without unnecessary energy consumption. Figure 5.12 (c) shows the influence of membrane permeance on LCOH. As the permeance increases, more hydrogen is selectively removed from the reaction zone, shifting the equilibrium forward and improving recovery. The sudden

decrease in LCOH at low flux values demonstrates the high sensitivity of the system to hydrogen separation efficiency. However, similar to the pressure and temperature trends, the effect begins to level off at higher permeances. This indicated that while membrane performance is critical, beyond a certain point, further improvements give limited economic benefits.

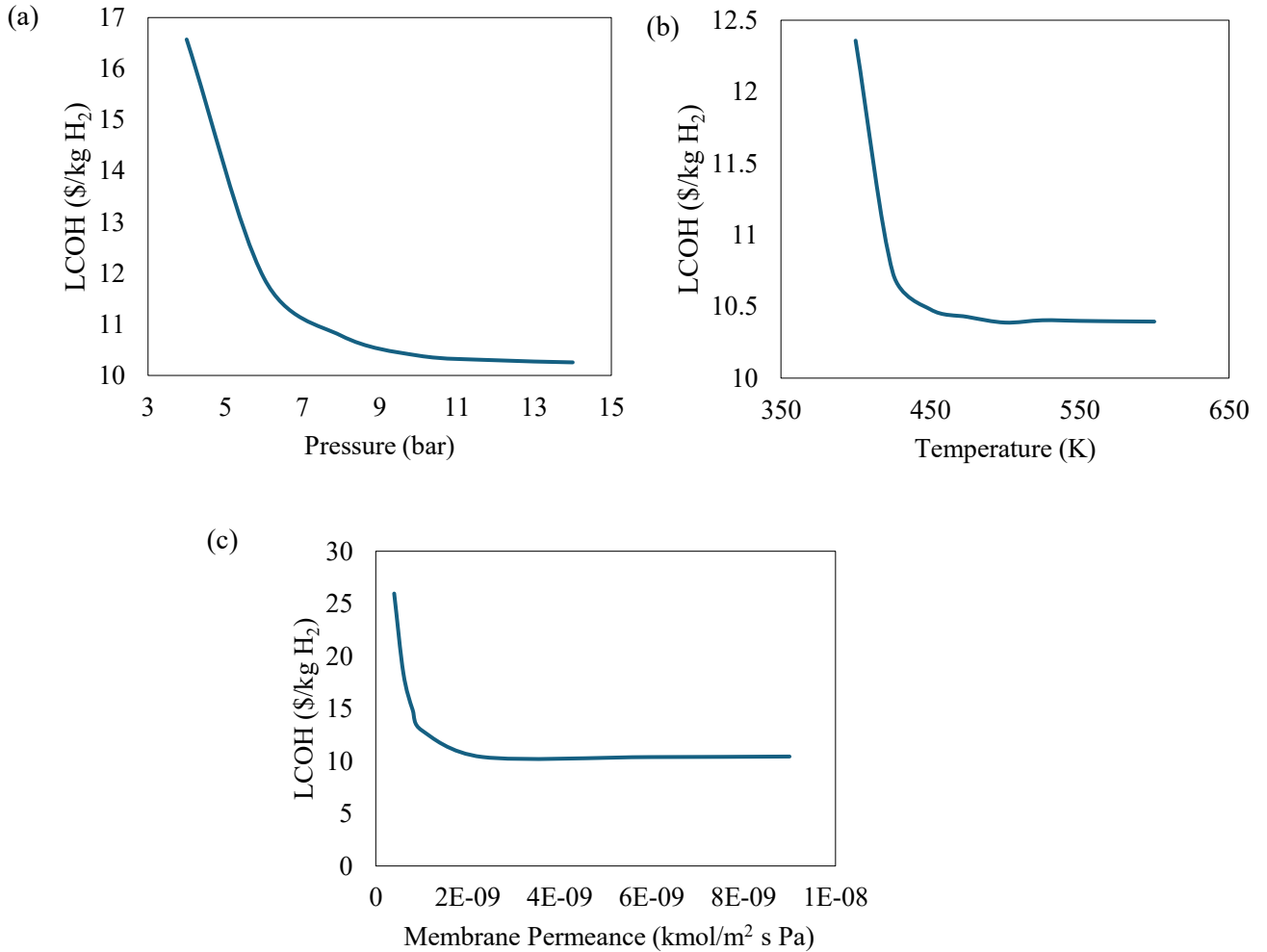


Figure 5.12: Effect of key parameters of LCOH.

Together, these results demonstrate that while pressure, temperature, and membrane permeance all play important roles in determining the LCOH, each exhibits a point of diminishing returns. Identifying and operating within these optimal ranges allows for an efficient, cost-effective design that maximizes hydrogen yield without incurring unnecessary energy or material costs.

# Chapter 6 Conclusions and Recommendations

This chapter summarizes the research done on designing an on-site hydrogen refuelling station and provides limitations and recommendations for future work.

## 5.1 Conclusion

In conclusion, this Master's thesis successfully demonstrates the design of a hydrogen refuelling station based on ammonia decomposition using a packed bed membrane reactor. Python-based modelling and simulation, primarily using the Cantera library, were applied to evaluate both technical performance and economic feasibility. This work contributes to the growing body of research on hydrogen production and provides a reproducible, transparent modelling framework.

Chapters 1 and 2 provided a foundational review of key concepts relevant to this study, including the fundamentals of ammonia decomposition, catalyst selection, and membrane technologies. The role of ammonia combustion and selective catalytic reduction (SCR) in hydrogen production systems was also discussed in the context of designing a complete refuelling station. Furthermore, techno-economic and environmental assessment frameworks were introduced to guide later analysis. A literature review summarized existing models and highlighted gaps in current research.

Chapter 3 detailed the methodology used to design and simulate the refuelling station. The system includes key components such as a pump, furnace, SCR unit, compressor, and multiple heat exchangers, all of which were modelled using Python and Cantera. A PBMR was designed using a nickel-based catalyst and validated against experimental data from Kogekar [30] at lab scale. The reactor was then scaled up to meet a daily hydrogen demand of 500 kg. Operating at 10 bar and 500 °C, the system achieved an ammonia conversion of 99.92% and a hydrogen recovery of 95.9%, with a minor pressure drop of 0.02 bar.

Chapter 4 focused on the techno-economic and environmental analysis of the base case. Capital and operating costs were estimated assuming constant design and operating parameters. The calculated Levelized Cost of Hydrogen (LCOH) was \$10.38/kg H<sub>2</sub>. The energy consumption for the system was 9.77 kWh/kg H<sub>2</sub>, with the majority of electricity demand coming from the compressor and the reactor's thermal maintenance. Although ammonia decomposition does not produce direct CO<sub>2</sub> emissions, indirect emissions were estimated based on Ontario's electricity grid mix, resulting in a total of 0.28 kg CO<sub>2</sub>e/kg H<sub>2</sub>. Additionally, NO<sub>x</sub> emissions generated during ammonia combustion were evaluated. The concentration of NO<sub>x</sub> after combustion was 0.09 µg/m<sup>3</sup>, which was reduced to 0.026 µg/m<sup>3</sup> after SCR treatment.

Chapter 5 explored the sensitivity of the reactor performance to key operating parameters: temperature, pressure, and membrane permeance. Results showed that higher values of these parameters improved ammonia conversion and hydrogen recovery while reducing specific energy consumption. Optimal performance was observed at 8–10 bar, 450–500 °C, and a membrane permeance of  $6 \times 10^{-9}$  kmol/m<sup>2</sup>·s·Pa. Additionally, the effect of equivalence ratio on NO<sub>x</sub> emissions from the combustion unit was examined. Increasing the equivalence ratio above one was shown to reduce NO<sub>x</sub> formation, with an optimal value of 1.2. A cost sensitivity analysis was also performed to assess the impact of capital and operating expenses on the LCOH. It was found that LCOH decreases as system efficiency increases and more hydrogen is produced. The ammonia feedstock cost was identified as the most influential economic factor, varying it by ±30% changed the LCOH from \$9.30 to \$11.50/kg H<sub>2</sub>. The second-largest cost driver was the compressor.

This study highlights the potential of ammonia as a hydrogen carrier for refuelling applications, and it provides a practical modelling approach to evaluate the technical and economic feasibility of such systems.

## **5.2 Limitations of the Study and Recommendations of Future Work**

In this thesis there are some limitations that should be acknowledged. First, the reactor and system were modelled in one dimension, which neglects radial heat and mass transfer effects present in real systems. In addition, combustion processes were approximated using basic reactor models without detailed treatment of flame dynamics.

To strengthen the robustness of this model, several areas of future work are proposed.

- (a) Future studies should explore multi-dimensional modelling to capture heat and mass transfer in radial directions, as well as non-ideal flow behaviours such as channelling and dead zones. In particular, detailed modelling of membrane transport and degradation mechanisms would improve performance predictions over time. Incorporating computational fluid dynamics (CFD) and detailed kinetic models could improve predictions of combustion efficiency, flame stability, and NO<sub>x</sub> formation. Studying the role of equivalence ratio, ammonia to hydrogen ratio (fuel), and burner design would support the development of clean ammonia combustion systems.
- (b) Expanding the model to include transient behaviour, such as during startup, shutdown, or load changes, would help simulate real-world operation. Integration with heat exchangers, storage, compression systems, and safety controls would support full system-level optimization.

- (c) As a next step toward commercialization, a pilot-scale demonstration should be considered in collaboration with industry. This would allow for validation of simulation results, testing of hardware and safety protocols, and refinement of process control strategies.

These future works should be done in the order suggested above. This work is important as society strives toward a greener and cleaner future.

## References

- [1] N. R. Canada, 'Clean Fuels Fund'. Accessed: Apr. 25, 2025. [Online]. Available: <https://natural-resources.canada.ca/energy-sources/clean-fuels/clean-fuels-fund>
- [2] E. and C. C. Canada, 'Greenhouse gas emissions'. Accessed: Apr. 25, 2025. [Online]. Available: <https://www.canada.ca/en/environment-climate-change/services/environmental-indicators/greenhouse-gas-emissions.html>
- [3] N. R. Canada, 'Energy from hydrogen: the basics'. Accessed: Apr. 25, 2025. [Online]. Available: <https://natural-resources.canada.ca/energy-sources/clean-fuels/energy-hydrogen-basics>
- [4] N. R. Canada, 'Hydrogen Strategy for Canada: Progress Report'. Accessed: Apr. 28, 2025. [Online]. Available: <https://natural-resources.canada.ca/energy-sources/clean-fuels/hydrogen-strategy/hydrogen-strategy-canada-progress-report>
- [5] 'Heat Values of Various Fuels', World Nuclear Association. Accessed: May 14, 2025. [Online]. Available: <https://world-nuclear.org/information-library/facts-and-figures/heat-values-of-various-fuels>
- [6] M. Joshi, I. Chernyakhovskiy, and M. Chung, 'Hydrogen 101: Frequently Asked Questions About Hydrogen for Decarbonization', National Renewable Energy Laboratory. Accessed: May 13, 2025. [Online]. Available: <https://docs.nrel.gov/docs/fy22osti/82554.pdf>
- [7] I. Iacob, M. G. Morgan, and S. Curtis, 'Barriers to Creating a Market for Hydrogen: Insights from Global Roadmaps and Stakeholders in the United States', *Energy Res. Soc. Sci.*, vol. 121, p. 103947, Mar. 2025, doi: 10.1016/j.erss.2025.103947.
- [8] X. Fan and Y. F. Cheng, 'Hydrogen pipelines and embrittlement in gaseous environments: An up-to-date review', *Appl. Energy*, vol. 387, p. 125636, Jun. 2025, doi: 10.1016/j.apenergy.2025.125636.
- [9] M. M. Hossain Bhuiyan and Z. Siddique, 'Hydrogen as an alternative fuel: A comprehensive review of challenges and opportunities in production, storage, and transportation', *Int. J. Hydrog. Energy*, vol. 102, pp. 1026–1044, Feb. 2025, doi: 10.1016/j.ijhydene.2025.01.033.
- [10] 'Molecule of the Week Archive: Ammonia', ACS Chemistry for Life. Accessed: May 14, 2025. [Online]. Available: <https://www.acs.org/molecule-of-the-week/archive/a/ammonia.html>
- [11] 'Ammonia', Chemical Safety Facts: Information on Chemicals in Everyday Products. Accessed: May 14, 2025. [Online]. Available: <https://www.chemicalsafetyfacts.org/chemicals/ammonia/>
- [12] A. Franco and C. Giovannini, 'Hydrogen Gas Compression for Efficient Storage: Balancing Energy and Increasing Density', *Hydrogen*, vol. 5, no. 2, pp. 293–311, May 2024, doi: 10.3390/hydrogen5020017.
- [13] G. Kubilay Karayel, N. Javani, and I. Dincer, 'A comprehensive assessment of energy storage options for green hydrogen', *Energy Convers. Manag.*, vol. 291, p. 117311, Sep. 2023, doi: 10.1016/j.enconman.2023.117311.
- [14] 'Storage & Handling - Anhydrous Ammonia', Tanner Industries Inc. Accessed: May 14, 2025. [Online]. Available:

[https://www.tannerind.com/PDF/Storage\\_%20Handling\\_NH\\_3\\_Rev\\_version\\_8.31.20.pdf](https://www.tannerind.com/PDF/Storage_%20Handling_NH_3_Rev_version_8.31.20.pdf)

- [15] V. Pattabathula, R. Nayak, and D. Timbres, 'Ammonia Storage Tanks'. Accessed: May 14, 2025. [Online]. Available: <https://ammoniaknowhow.com/ammonia-storage-tanks/>
- [16] 'Zero Emission Vehicle Infrastructure Program funding – Indigenous organizations', Government of Canada. Accessed: May 15, 2025. [Online]. Available: <https://natural-resources.canada.ca/energy-efficiency/transportation-energy-efficiency/zero-emission-vehicle-infrastructure/zevip-indigenous-organizations>
- [17] D. A. Cullen *et al.*, 'New roads and challenges for fuel cells in heavy-duty transportation'. [Online]. Available: <https://www.osti.gov/servlets/purl/1777401>
- [18] 'Electric Charging and Alternative Fuelling Stations Locator', Government of Canada. Accessed: May 15, 2025. [Online]. Available: <https://natural-resources.canada.ca/energy-efficiency/transportation-energy-efficiency/electric-charging-alternative-fuelling-stationslocator-map#/find/nearest?fuel=HY>
- [19] B. Lee, J. Park, H. Lee, M. Byun, C. W. Yoon, and H. Lim, 'Assessment of the economic potential: CO<sub>2</sub>-free hydrogen production from renewables via ammonia decomposition for small-sized H<sub>2</sub> refueling stations', *Renew. Sustain. Energy Rev.*, vol. 113, p. 109262, Oct. 2019, doi: 10.1016/j.rser.2019.109262.
- [20] S. Pardhi, S. Chakraborty, D.-D. Tran, M. El Baghdadi, S. Wilkins, and O. Hegazy, 'A Review of Fuel Cell Powertrains for Long-Haul Heavy-Duty Vehicles: Technology, Hydrogen, Energy and Thermal Management Solutions', *Energies*, vol. 15, no. 24, p. 9557, Dec. 2022, doi: 10.3390/en15249557.
- [21] F. Liu, D. L. Mauzerall, F. Zhao, and H. Hao, 'Deployment of fuel cell vehicles in China: Greenhouse gas emission reductions from converting the heavy-duty truck fleet from diesel and natural gas to hydrogen', *Int. J. Hydrog. Energy*, vol. 46, no. 34, pp. 17982–17997, May 2021, doi: 10.1016/j.ijhydene.2021.02.198.
- [22] P. D. Larson, R. V. Parsons, and D. Kalluri, 'Zero-Emission Heavy-Duty, Long-Haul Trucking: Obstacles and Opportunities for Logistics in North America', *Logistics*, vol. 8, no. 3, p. 64, Jun. 2024, doi: 10.3390/logistics8030064.
- [23] Z. Su *et al.*, 'Research progress of ruthenium-based catalysts for hydrogen production from ammonia decomposition', *Int. J. Hydrog. Energy*, vol. 51, pp. 1019–1043, Jan. 2024, doi: 10.1016/j.ijhydene.2023.09.107.
- [24] R. Sitar, A. D'Aquila, J. L. Jechura, and C. A. Wolden, 'Techno-economic analysis of zero-carbon ammonia-hydrogen fuel blend production through a catalytic membrane reformer and packed bed reactor', *Renew. Sustain. Energy Rev.*, vol. 199, p. 114469, Jul. 2024, doi: 10.1016/j.rser.2024.114469.
- [25] J. B. Hansen, 'Kinetics of Ammonia Synthesis and Decomposition on Heterogeneous Catalysts', in *Ammonia*, A. Nielsen, Ed., Berlin, Heidelberg: Springer Berlin Heidelberg, 1995, pp. 149–190. doi: 10.1007/978-3-642-79197-0\_4.
- [26] I. Lucentini, X. Garcia, X. Vendrell, and J. Llorca, 'Review of the Decomposition of Ammonia to Generate Hydrogen', *Ind. Eng. Chem. Res.*, vol. 60, no. 51, pp. 18560–18611, Dec. 2021, doi: 10.1021/acs.iecr.1c00843.

- [27] F. Gallucci, E. Fernandez, P. Corengia, and M. Van Sint Annaland, 'Recent advances on membranes and membrane reactors for hydrogen production', *Chem. Eng. Sci.*, vol. 92, pp. 40–66, Apr. 2013, doi: 10.1016/j.ces.2013.01.008.
- [28] W. Wang *et al.*, 'Inorganic membranes for in-situ separation of hydrogen and enhancement of hydrogen production from thermochemical reactions', *Renew. Sustain. Energy Rev.*, vol. 160, p. 112124, May 2022, doi: 10.1016/j.rser.2022.112124.
- [29] R. Sitar, J. Shah, J. D. Way, and C. A. Wolden, 'Efficient Generation of H<sub>2</sub>/NH<sub>3</sub> Fuel Mixtures for Clean Combustion', *Energy Fuels*, vol. 36, no. 16, pp. 9357–9364, Aug. 2022, doi: 10.1021/acs.energyfuels.2c01822.
- [30] R. Sitar, J. Shah, Z. Zhang, H. Wikoff, J. D. Way, and C. A. Wolden, 'Compact ammonia reforming at low temperature using catalytic membrane reactors', *J. Membr. Sci.*, vol. 644, p. 120147, Feb. 2022, doi: 10.1016/j.memsci.2021.120147.
- [31] V. Cechetto, L. Di Felice, J. A. Medrano, C. Makhloufi, J. Zuniga, and F. Gallucci, 'H<sub>2</sub> production via ammonia decomposition in a catalytic membrane reactor', *Fuel Process. Technol.*, vol. 216, p. 106772, Jun. 2021, doi: 10.1016/j.fuproc.2021.106772.
- [32] S. Richard, A. R. Santos, P. Olivier, and F. Gallucci, 'Techno-economic analysis of ammonia cracking for large scale power generation', *Int. J. Hydrog. Energy*, vol. 71, pp. 571–587, 2024, doi: <https://doi.org/10.1016/j.ijhydene.2024.05.308>.
- [33] R. Nasharuddin, M. Zhu, Z. Zhang, and D. Zhang, 'A technoeconomic analysis of centralised and distributed processes of ammonia dissociation to hydrogen for fuel cell vehicle applications', *Int. J. Hydrog. Energy*, vol. 44, no. 28, pp. 14445–14455, May 2019, doi: 10.1016/j.ijhydene.2019.03.274.
- [34] J. Zhang, H. Xu, and W. Li, 'High-purity CO<sub>x</sub>-free H<sub>2</sub> generation from NH<sub>3</sub> via the ultra permeable and highly selective Pd membranes', *J. Membr. Sci.*, vol. 277, no. 1–2, pp. 85–93, Jun. 2006, doi: 10.1016/j.memsci.2005.10.014.
- [35] Z. Zhang, S. Liguori, T. F. Fuerst, J. D. Way, and C. A. Wolden, 'Efficient Ammonia Decomposition in a Catalytic Membrane Reactor To Enable Hydrogen Storage and Utilization', *ACS Sustain. Chem. Eng.*, vol. 7, no. 6, pp. 5975–5985, Mar. 2019, doi: 10.1021/acssuschemeng.8b06065.
- [36] G. M. Kogekar, 'Computationally efficient and robust models of non-ideal thermodynamics, gas-phase kinetics and heterogeneous catalysis in chemical reactors'.
- [37] R. Y. Chein, Y. C. Chen, and J. N. Chung, 'Sweep gas flow effect on membrane reactor performance for hydrogen production from high-temperature water-gas shift reaction', *J. Membr. Sci.*, vol. 475, pp. 193–203, Feb. 2015, doi: 10.1016/j.memsci.2014.09.046.
- [38] N. Realpe *et al.*, 'Modeling-aided coupling of catalysts, conditions, membranes, and reactors for efficient hydrogen production from ammonia', *React. Chem. Eng.*, vol. 8, no. 5, pp. 989–1004, 2023, doi: 10.1039/D2RE00408A.
- [39] C. Liu, X. Zhang, J. Zhai, X. Li, X. Guo, and G. He, 'Research progress and prospects on hydrogen separation membranes', *Clean Energy*, vol. 7, no. 1, pp. 217–241, Feb. 2023, doi: 10.1093/ce/zkad014.

- [40] G. Li, M. Kanezashi, T. Yoshioka, and T. Tsuru, 'Ammonia decomposition in catalytic membrane reactors: Simulation and experimental studies', *AIChE J.*, vol. 59, no. 1, pp. 168–179, 2013, doi: 10.1002/aic.13794.
- [41] H. Kobayashi, A. Hayakawa, K. D. K. A. Somarathne, and E. C. Okafor, 'Science and technology of ammonia combustion', *Proc. Combust. Inst.*, vol. 37, no. 1, pp. 109–133, 2019, doi: 10.1016/j.proci.2018.09.029.
- [42] C. Mounaïm-Rousselle, 'Principles of Ammonia combustion', [Online]. Available: <https://hal.science/hal-03519313/file/activate1.pdf>
- [43] S. Devkota *et al.*, 'Process design and optimization of onsite hydrogen production from ammonia: Reactor design, energy saving and NOX control', *Fuel*, vol. 342, p. 127879, Jun. 2023, doi: 10.1016/j.fuel.2023.127879.
- [44] H. S. Latha, K. V. Prakash, M. Veerangouda, D. Maski, and K. T. Ramappa, 'A Review on SCR System for NOx Reduction in Diesel Engine', *Int. J. Curr. Microbiol. Appl. Sci.*, vol. 8, no. 04, pp. 1553–1559, Apr. 2019, doi: 10.20546/ijcmas.2019.804.180.
- [45] Z. Shi *et al.*, 'Mechanism, performance and modification methods for NH<sub>3</sub>-SCR catalysts: A review', *Fuel*, vol. 331, p. 125885, Jan. 2023, doi: 10.1016/j.fuel.2022.125885.
- [46] D. C. Mussatti, 'The EPA Air Pollution Control Cost Manual', U.S. Environmental Protection Agency Office of Air Quality Planning and Stand, Final 452/B-02–001, Jan. 2002. Accessed: May 25, 2025. [Online]. Available: <https://www.epa.gov/sites/default/files/2020-07/documents/cs4-2ch2.pdf>
- [47] 'Air Pollution Control Technology Fact Sheet', United States Environmental Protection Agency. Accessed: May 29, 2025. [Online]. Available: <https://www3.epa.gov/ttnecatc1/dir1/fscr.pdf>
- [48] R. Turton, Ed., *Analysis, synthesis, and design of chemical processes*, 5th edition. in Prentice Hall international series in the physical and chemical engineering sciences. Boston: Prentice Hall, 2018.
- [49] C. Makhloufi and N. Kezibri, 'Large-scale decomposition of green ammonia for pure hydrogen production', *Int. J. Hydrog. Energy*, vol. 46, no. 70, pp. 34777–34787, Oct. 2021, doi: 10.1016/j.ijhydene.2021.07.188.
- [50] S. Devkota *et al.*, 'Techno-economic and environmental assessment of hydrogen production through ammonia decomposition', *Appl. Energy*, vol. 358, p. 122605, Mar. 2024, doi: 10.1016/j.apenergy.2023.122605.
- [51] E. Curcio, 'Techno-economic analysis of hydrogen production: Costs, policies, and scalability in the transition to net-zero', *Int. J. Hydrog. Energy*, vol. 128, pp. 473–487, May 2025, doi: 10.1016/j.ijhydene.2025.04.013.
- [52] S. Mashruk *et al.*, 'Perspectives on NO<sub>x</sub> Emissions and Impacts from Ammonia Combustion Processes', *Energy Fuels*, vol. 38, no. 20, pp. 19253–19292, Oct. 2024, doi: 10.1021/acs.energyfuels.4c03381.
- [53] 'Guideline A-9: NOx Emissions from Boilers and Heaters', Ontario. Accessed: May 15, 2025. [Online]. Available: <https://www.ontario.ca/page/guideline-9-nox-emissions-boilers-and-heaters>
- [54] 'O. Reg. 419/05: AIR POLLUTION - LOCAL AIR QUALITY', Ontario. Accessed: May 15, 2025. [Online]. Available: <https://www.ontario.ca/laws/regulation/050419>

- [55] ‘Ontario energy snapshot’, Ontario. [Online]. Available: <https://www.ontario.ca/page/ontario-energy-snapshot#:~:text=Ontario%20has%20one%20of%20the,continue%20using%20natural%20gas%20to:>.
- [56] D. G. Goodwin, H. K. Moffat, I. Schoegl, R. L. Speth, and B. W. Weber, *Cantera: An Object-oriented Software Toolkit for Chemical Kinetics, Thermodynamics, and Transport Processes*. (Dec. 14, 2024). Zenodo. doi: 10.5281/ZENODO.14455267.
- [57] B. Malengier, P. Kišon, J. Tocknell, C. Abert, F. Bruckner, and M.-A. Bisotti, ‘ODES: a high level interface to ODE and DAE solvers’, *J. Open Source Softw.*, vol. 3, no. 22, p. 165, Feb. 2018, doi: 10.21105/joss.00165.
- [58] H. Zhu, C. Karakaya, and R. J. Kee, ‘Modeling ammonia-fueled co-flow dual-channel protonic-ceramic fuel cells’, *Int. J. Green Energy*, vol. 19, no. 14, pp. 1568–1582, Nov. 2022, doi: 10.1080/15435075.2021.2018321.
- [59] Z. Zhang, C. Karakaya, R. J. Kee, J. D. Way, and C. A. Wolden, ‘Barium-Promoted Ruthenium Catalysts on Yttria-Stabilized Zirconia Supports for Ammonia Synthesis’, *ACS Sustain. Chem. Eng.*, vol. 7, no. 21, pp. 18038–18047, Nov. 2019, doi: 10.1021/acssuschemeng.9b04929.
- [60] F. H. Marques and R. Guirardello, ‘Gibbs energy minimization with cubic equation of state and Henry’s law to calculate thermodynamic equilibrium of Fischer-Tropsch synthesis’, *Fluid Phase Equilibria*, vol. 502, p. 112290, Dec. 2019, doi: 10.1016/j.fluid.2019.112290.
- [61] G. D. Ulrich and P. T. Vasudevan, *Chemical engineering: process design and economics ; a practical guide*, 2nd ed. Durham, NH: Process Publ, 2004.
- [62] C. Maxwell, ‘Cost Indices’, Towering Skills. [Online]. Available: <https://toweringskills.com/financial-analysis/cost-indices/>
- [63] ‘Ammonia price index’, Business Analytiq. [Online]. Available: <https://businessanalytiq.com/procurementanalytics/index/ammonia-price-index/>
- [64] ‘Current water rates’, Peel Region. [Online]. Available: <https://peelregion.ca/water/water-billing/rates-charges/current-water-rates>
- [65] ‘Water Rates & Fees’, Toronto. [Online]. Available: <https://www.toronto.ca/services-payments/property-taxes-utilities/utility-bill/water-rates-fees/>
- [66] ‘Water and sewer rates’, Kitchener Utilities. [Online]. Available: <https://www.kitchenerutilities.ca/en/rates/water-and-sewer-rates.aspx#>
- [67] ‘Electricity rates’, Ontario Energy Board. [Online]. Available: <https://www.oeb.ca/consumer-information-and-protection/electricity-rates>
- [68] M. Ongis, M. Baiguini, G. Di Marcoberardino, F. Gallucci, and M. Binotti, ‘Techno-economic analysis for the design of membrane reactors in a small-scale biogas-to-hydrogen plant’, *Int. J. Hydrog. Energy*, vol. 101, pp. 887–903, Feb. 2025, doi: 10.1016/j.ijhydene.2024.12.245.
- [69] J. L. Sorrels, D. D. Randall, C. R. Fry, and K. S. Shaffner, ‘Selective Catalytic Reduction’, June 19. [Online]. Available: [https://www.epa.gov/sites/default/files/2017-12/documents/scrcostmanualchapter7thedition\\_2016revisions2017.pdf](https://www.epa.gov/sites/default/files/2017-12/documents/scrcostmanualchapter7thedition_2016revisions2017.pdf)

- [70] 'Chemical Operator, Chemical-processing in Ontario', Government of Canada. [Online]. Available: <https://www.jobbank.gc.ca/marketreport/wages-occupation/20513/ON;jsessionid=5BF4FA456E5AF93BFE8BB967A3509FAD.jobse arch76>
- [71] 'Station Status', HTEC Fueling the drive to hydrogen. [Online]. Available: <https://www.htec.ca/status/>
- [72] 'Hydrogen Prices at USA Stations', ECO vehicles. [Online]. Available: <https://www.glpautogas.info/en/hydrogen-sale-price-united-states.html>
- [73] R. Dickson, M. S. Akhtar, A. Abbas, E. D. Park, and J. Liu, 'Global transportation of green hydrogen *via* liquid carriers: economic and environmental sustainability analysis, policy implications, and future directions', *Green Chem.*, vol. 24, no. 21, pp. 8484–8493, 2022, doi: 10.1039/D2GC02079C.
- [74] H. Noh, K. Kang, and Y. Seo, 'Environmental and energy efficiency assessments of offshore hydrogen supply chains utilizing compressed gaseous hydrogen, liquefied hydrogen, liquid organic hydrogen carriers and ammonia', *Int. J. Hydrog. Energy*, vol. 48, no. 20, pp. 7515–7532, Mar. 2023, doi: 10.1016/j.ijhydene.2022.11.085.
- [75] E. Bianco, D. Hawila, and H. Blanco, *Green Hydrogen Supply: A Guide to Policy Making*. International Renewable Energy Agency, 2021. [Online]. Available: [https://h2chile.cl/wp-content/uploads/2024/02/IRENA\\_Green\\_Hydrogen\\_Supply\\_2021.pdf](https://h2chile.cl/wp-content/uploads/2024/02/IRENA_Green_Hydrogen_Supply_2021.pdf)
- [76] W. Stafford, V. Russo, K. Chaba, and T. Goga, 'Carbon intensity of green ammonia as a fuel for maritime transport', presented at the Life Cycle Innovation Conference, Berlin, Germany, 2024. [Online]. Available: <https://fslci.org/lcic/lcic2024/lcic2024-abstracts/carbon-intensity-of-green-ammonia-as-a-fuel-for-maritime-transport/>
- [77] H. H. Cho, V. Strezov, and T. J. Evans, 'Life cycle assessment of renewable hydrogen transport by ammonia', *Int. J. Hydrog. Energy*, vol. 94, pp. 1018–1035, Dec. 2024, doi: 10.1016/j.ijhydene.2024.11.076.
- [78] A. O. Oni, K. Anaya, T. Giwa, G. Di Lullo, and A. Kumar, 'Comparative assessment of blue hydrogen from steam methane reforming, autothermal reforming, and natural gas decomposition technologies for natural gas-producing regions', *Energy Convers. Manag.*, vol. 254, p. 115245, Feb. 2022, doi: 10.1016/j.enconman.2022.115245.
- [79] M. Katebah, M. Al-Rawashdeh, and P. Linke, 'Analysis of hydrogen production costs in Steam-Methane Reforming considering integration with electrolysis and CO<sub>2</sub> capture', *Clean. Eng. Technol.*, vol. 10, p. 100552, Oct. 2022, doi: 10.1016/j.clet.2022.100552.
- [80] G. Gonzales-Calienes, M. Kannangara, J. Yang, J. Shadbahr, C. Deces-Petit, and F. Bensebaa, 'LIFE CYCLE ASSESSMENT OF HYDROGEN PRODUCTION PATHWAYS IN CANADA', National Research Council Canada, 2022. Accessed: Jun. 16, 2025. [Online]. Available: [https://publications.gc.ca/collections/collection\\_2022/cnrc-nrc/NR16-399-2022-eng.pdf](https://publications.gc.ca/collections/collection_2022/cnrc-nrc/NR16-399-2022-eng.pdf)
- [81] S. Consonni, L. Mastropasqua, M. Spinelli, T. A. Barckholtz, and S. Campanari, 'Low-carbon hydrogen via integration of steam methane reforming with molten

carbonate fuel cells at low fuel utilization', *Adv. Appl. Energy*, vol. 2, p. 100010, May 2021, doi: 10.1016/j.adapen.2021.100010.

- [82] 'Comparison of the emissions intensity of different hydrogen production routes, 2021', iea. Accessed: Jun. 16, 2025. [Online]. Available: <https://www.iea.org/data-and-statistics/charts/comparison-of-the-emissions-intensity-of-different-hydrogen-production-routes-2021>

# Appendix A

Table A.1: Base case stream results

Parameters	S1	S2	S3	S4	S5	S6	S7	S8	S9	S10
Temperature (K)	239.15	239.353	301.15	301.15	773.15	773.15	753.15	323.15	298.15	773.15
Pressure (Pa)	101325	1000000	1000000	1000000	1000000	100000	100000	100000	35000000	998815.5
NH <sub>3</sub>	1	1	1	1	1	0	0	0	0	0.000994
N <sub>2</sub>	0	0	0	0	0	0	0	0	0	0.990245
H <sub>2</sub>	0	0	0	0	0	1	1	1	1	0.008761
Ar	0	0	0	0	0	0	0	0	0	0
O <sub>2</sub>	0	0	0	0	0	0	0	0	0	0
H <sub>2</sub> O	0	0	0	0	0	0	0	0	0	0
NO	0	0	0	0	0	0	0	0	0	0
NO <sub>2</sub>	0	0	0	0	0	0	0	0	0	0
N <sub>2</sub> O	0	0	0	0	0	0	0	0	0	0
Mass Flowrate (kg/s)	0.0361	0.0361	0.0361	0.034	0.034	0.005785	0.005785	0.005785	0.005784845	0.028215

Parameters	S11	S12	S13	S14	S15	S16	S17	S18	S19	S20
Temperature (K)	301.15	639.4532	333.15	313.15	1339.308	638.3426	293.15	329.1258	329.1258	329.1258
Pressure (Pa)	1000000	1000000	100000	100000	1000000	1000000	1000000	1000000	1000000	1000000
NH <sub>3</sub>	1	1	0	0	1.04E-05	1.04E-05	0	0	0	0
N <sub>2</sub>	0	0	0.7554	0.7554	0.910021	0.910021	0.7554	0.7554	0.7554	0.7554
H <sub>2</sub>	0	0	0	0	0.005084	0.005084	0	0	0	0
Ar	0	0	0.013	0.013	0.004257	0.004257	0.013	0.013	0.013	0.013
O <sub>2</sub>	0	0	0.231	0.231	1.18E-14	1.18E-14	0.231	0.231	0.231	0.231
H <sub>2</sub> O	0	0	0	0	0.080628	0.080628	0	0	0	0
NO	0	0	0	0	1.3E-10	1.3E-10	0	0	0	0
NO <sub>2</sub>	0	0	0	0	1.23E-18	1.23E-18	0	0	0	0
N <sub>2</sub> O	0	0	0	0	4.01E-14	4.01E-14	0	0	0	0
Mass Flowrate (kg/s)	0.002077	0.002077	2.647295	2.647295	0.044009	0.044009	1	1	0.013717	0.986283

Parameters	S11	S12
Temperature (K)	329.1258	638.3426
Pressure (Pa)	1000000	1000000
NH <sub>3</sub>	0	1.04E-05
N <sub>2</sub>	0.7554	0.910021
H <sub>2</sub>	0	0.005084
Ar	0.013	0.004257
O <sub>2</sub>	0.231	1.45E-07
H <sub>2</sub> O	0	0.080627
NO	0	1.95E-11
NO <sub>2</sub>	0	2.77E-20
N <sub>2</sub> O	0	4.01E-14
Mass Flowrate (kg/s)	6.4E-09	0.044009

Table A.2: Base case pump results Python model vs the Aspen Plus model.

Assuming 70% isentropic efficiency

Parameter	Python Model Results	Aspen Plus Model Results	Percent Error (%)
Power Actual (W)	67.55848	67.7139103	0.22954
Power Theoretical (W)	47.29093	47.3997372	0.22955

Table A.3: Base case heat exchanger with phase change results Python model vs the Aspen Plus model.

Parameter	Python Model Results	Aspen Plus Model Results	Percent Error (%)
Duty Exchange	53238.51	53696.353	0.852652
Zone 1 Heat (W)	9489.163	9926.43	4.405078
Zone 2 Heat (W)	43535.41	43535.8	0.000896
Zone 3 Heat (W)	213.93	234.112	8.62066
Total Area	2.529672	2.28404195	10.75418

Table A.4: Base case heat exchangers (Ex: HX4) results Python model vs the Aspen Plus model.

Parameter	Python Model Results	Aspen Plus Model Results	Percent Error (%)
Duty Exchange	36128.14	36283.581808884	0.428408
Tout (hot fluid)	329.1258	328.409	0.218264
LMTD	148.7673	148.943	0.117965
Area	0.285706	0.286597	0.31089

Table A.5: Base case multistage compressor results Python model vs the Aspen Plus model.

Parameter	Python Model Results	Aspen Plus Model Results	Percent Error (%)
Total Work (W)	98376.2	100661.182	2.269973
Total Cooling (W)	99644.36	101931.044	2.243364

Table A.6: Base case ammonia combustion results Python model vs the Aspen Plus model.

Assuming an equivalence ratio of 0.94.

Parameter	Python Model Results	Aspen Plus Model Results	Percent Error (%)
Temperature Out	1373.5738	1373.25867	0.022948
NH <sub>3</sub>	7.596e-06	7.7267E-06	1.691537
N <sub>2</sub>	9.138e-01	0.91384167	0.00456
H <sub>2</sub>	4.456e-03	0.00445446	0.034572
Ar	0.000e+00	0.0	0
O <sub>2</sub>	4.804e-14	4.73711E-14	1.412042
H <sub>2</sub> O	8.169e-02	0.08169614	0.007516
NO	3.232e-10	3.46634E-10	6.760445
NO <sub>2</sub>	5.434e-18	5.54151E-18	1.940085
N <sub>2</sub> O	9.862e-14	9.25022E-14	6.613681

Table A.7: Energy Consumption for hydrogen production processes.

Note: 4.7 kWh/kg H<sub>2</sub> was added to each process to ensure consistency of the hydrogen output, as compression consumes a lot of energy.

Process	Average kWh/kg H <sub>2</sub>	Range kWh/kg H <sub>2</sub>	Resources
Ammonia Decomposition with membrane (thesis work)	9.77	-	Current thesis base case results
Ammonia Decomposition without membrane	10.3		[77]
SMR	4.82-5.68	0.1-0.96 +4.72	[78], [79]
SOEC electrolyzers	44.7		[75]
Alkaline & PEM electrolyzers	54.7		[75]

Table A.8: CO<sub>2</sub> emissions for hydrogen production processes.

Process	kg CO <sub>2</sub> e/kg H <sub>2</sub>	Resources
Ammonia Decomposition with membrane	4.86	Current thesis base case results
Ammonia Decomposition with PSA	5.24	[50]
SMR	11.4	[80],[81]
SMR with CCS 60%	6	[82]
SMR with CCS 93%	3.7	[82]
Coal Gasification	22.7	[82]
Coal Gasification with CCS 93%	3.1	[82]
Coal Gasification with CCS 98%	2.3	[82]
Electrolysis 2021 global grid	23.5	[82]
Electrolysis nuclear power	0.2	[82]
Electrolysis wind	4.10	[82]
Electrolysis solar	3.6	[82]

Table A.9: Total Equipment Cost (CAD).

Equipment	Detail	Size	2004 Cost (CEPCI=400)	2024 Cost (CEPCI=798.8)
Pump	Centrifugal	shaft power=0.07 kW	1800	3594.6
HX1	Double pipe	2.5 m <sup>2</sup>	2200	4393.4
HX3	Double pipe	0.01 m <sup>2</sup>	800	1597.6
HX4	Double pipe	0.3 m <sup>2</sup>	1600	3195.2
Reactor	Horizontal vessel	L=1.6 and Diameter=0.8m	2500	4992.5
SCR	Horizontal vessel	L=1.2m and Diameter=0.3m	1000	1997
Combustion	HX2+Vertical vessel		1800	3594.6
Compressor	Centrifugal	fluid power 98kW	80000	159760
Ammonia storage cost	Found cost online for 10000 gallon tank			20661.42